CHEMISTRY OF MATERIALS

pubs.acs.org/cm

Article

Surfactant-Free Colloidal Syntheses of Gold-Based Nanomaterials in Alkaline Water and Mono-alcohol Mixtures

Jonathan Quinson,* Olivia Aalling-Frederiksen, Waynah L. Dacayan, Joachim D. Bjerregaard, Kim D. Jensen, Mads R. V. Jørgensen, Innokenty Kantor, Daniel R. Sørensen, Luise Theil Kuhn, Matthew S. Johnson, María Escudero-Escribano, Søren B. Simonsen, and Kirsten M. Ø. Jensen*

Cite This: *Chem. Mater.* 2023, 35, 2173–2190

Read Online

ACCESS | Metrics & More | Article Recommendations | Supporting Information

ABSTRACT: Gold nanoparticles (Au NPs) and gold-based nanomaterials combine unique properties relevant for medicine, imaging, optics, sensing, catalysis, and energy conversion. While the Turkevich–Frens and Brust–Schiffrin methods remain the state-of-the-art colloidal syntheses of Au NPs, there is a need for more sustainable and tractable synthetic strategies leading to new model systems. In particular, stabilizers are almost systematically used in colloidal syntheses, but they can be detrimental for fundamental and applied studies. Here, a surfactant-free synthesis of size-controlled colloidal Au NPs stable for months is achieved by the simple reduction of $HAuCl_4$ at room temperature in alkaline solutions of low-viscosity mono-alcohols such as ethanol or methanol and water, without the need for any other additives. Palladium (Pd) and bimetallic Au_xPd_y NPs, nanocomposites and multimetallic samples, are also obtained and are readily active (electro)catalysts. The multiple benefits over the state-of-the-art syntheses that this simple synthesis bears for fundamental and applied research are highlighted.

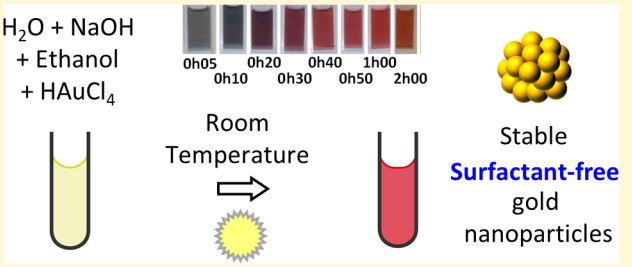

INTRODUCTION

Gold (Au)-based nanomaterials (NMs) are used in applications ranging from biomedical diagnostics and treatments to imaging and catalysis.[1−3] A crucial achievement for a successful Au-based nanotechnology is the controlled synthesis of nanoparticles (NPs) at sizes below 100 nm. Numerous syntheses have been reported, and interested readers will find numerous reviews of the synthesis of Au NPs[4] with an increasing focus on developing more sustainable syntheses.[5,6] In particular, wet-chemical colloidal syntheses in which a gold molecular precursor is converted into Au NPs by reduction in the liquid phase are widely used, typically in the presence of stabilizers such as surfactants and at relatively low concentrations.[4] Examples of surfactant-based colloidal syntheses are summarized in Table 1. The state-of-the-art colloidal syntheses of Au NPs remain the Turkevich–Frens method,[7,8] performed in close-to-boiling water using trisodium citrate (Na_3Ct) as a reducing and protecting agent, and the Brust–Schiffrin method,[9] performed at room temperature (RT) in organic media using $NaBH_4$ as a reducing agent and thiol-based compounds as stabilizers.

Overall, Au NP syntheses often require organic solvents and/or strong and hazardous reducing agents.[12] There is thus an interest in developing cheaper and more sustainable methods. Water-based strategies facilitate scaling by minimizing organic and hazardous waste. RT syntheses are possible due to the high reduction potentials of Au precursors and are appealing for large scale production as they minimize hazards and cost.[6,17] A range of RT syntheses in alcohols (ROHs) such as polyols are typically performed under alkaline conditions to facilitate the reduction of the metal precursor by the formation of alkoxides.[18] RT syntheses using plant extracts and/or (micro)organisms are possible in aqueous media.[13,14] However, impurities in these bioderived compounds can be challenging to control, and different feedstocks and/or purification processes can lead to different Au NP properties.[19] Furthermore, due to the rich chemistry of biomolecules, it is challenging to identify the functional group(s) responsible for the reduction of the gold precursor, which might impair further optimization of the synthesis.[19]

More reagents also mean more potential sources of impurities, leading to irreproducibility and unwarranted complexity for the synthesis.[20] In addition, while the use of additives and surfactants is claimed to be necessary to achieve colloidal stability, size, and/or shape control, surfactants are often not desirable for most applications. Surfactant removal is typically required, in catalysis to optimize the availability of

Received: January 13, 2023
Revised: February 10, 2023
Published: February 24, 2023

https://doi.org/10.1021/acs.chemmater.3c00090
Chem. Mater. 2023, 35, 2173–2190

Table 1. Overview of Colloidal Au NP Synthetic Strategies

type	ref	solvent	reducing agent	*green* solvent? (see ref 10)	*green* reducing agent? (see refs 10 and 11)	surfactant-free[a]	low-T_{bp} solvent (≤100 °C)	RT
Turkevich−Frens	7, 8	water	Na_3Ct	yes	no	no	yes	no
Brust−Schiffrin	9	toluene, water	$NaBH_4$	no	no	no	no	yes
DMF[b]	12	DMF	DMF	no	no	yes	no	no
biogenic	13	water	biomolecules (e.g., from plants)	yes	yes	no	yes	yes
microorganisms	14	water	microorganisms	yes	yes	no	yes	yes
polyols (e.g., glycerol)	15	polyols with water	polyols	yes	yes	yes	no	yes
mono-alcohols	this work	mono-alcohol(s) (with water)	mono-alcohols	yes	yes	yes	yes	yes

[a]Or free of additives other than solvents or reducing agents or "is the reducing agent a simple molecule with a molar mass of <100 g mol^{-1}?" [b]*N,N*-Dimethylformamide.

active surface sites[21] and in medicine to best functionalize NPs with desired molecules.[22] Surfactant removal involves chemical or physical treatments, e.g., a high temperature,[21] that are typically only moderately successful and challenging to scale. While often deemed impossible, surfactant-free syntheses of colloidal precious metal (PM) NPs can be achieved.[23] To the best of our knowledge, there is no consensus on the definition of a surfactant-free synthesis.[23−25] We here considered that a synthesis is surfactant-free if no species other than the metal precursor has a molar mass of >100 g mol^{-1}.[23] Polyols in alkaline solutions,[26] e.g., in glycerol for Au NPs,[15] are examples of suitable reductants for surfactant-free PM NP syntheses. It is believed that the high viscosity of the polyols accounts for the stabilization of the NPs. Unfortunately, the high viscosity of polyols prevents a simple use of the as-prepared NPs.[27] It has recently been show that mono-alcohols could lead to stable surfactant-free colloidal NPs under alkaline conditions, such as Pt,[28] Ir,[28,29] Ru,[28] or Os[30,31] NPs even at high precursor concentrations around 50 mM and at temperatures close to the boiling point of methanol (∼65 °C) or ethanol (∼78 °C).

However this approach does not easily lead to stable colloidal Pd NPs that are best prepared at RT in the presence of a support.[32] Equally, this approach does not lead to Au NPs. Due to the high reduction potentials of $Pd(NO_3)_2$ and $HAuCl_4$, using alkaline methanol or ethanol as a reducing agent leads, at RT, to large and/or agglomerated materials in the micrometer to millimeter range but not to colloidal surfactant-free NPs. Obtaining stable surfactant-free Au NPs with size control using mono-alcohols as the reducing agent therefore remained a daunting challenge. Nevertheless, inspired by the possibility of developing surfactant-free yet stable colloidal NPs of PMs using mono-alcohols as reducing agents, the hypothesis driving the work presented here is that carefully controlling the reaction conditions for Au NP synthesis, e.g., lower concentration of the precursor and fine balance between the amount of base and the amount of reducing agent, could lead to stable surfactant-free colloidal Au NPs.

An ultimate, scalable and *green* synthesis of Au NPs would be (i) surfactant-free and carried out (ii) at RT, (iii) in aqueous media, and (iv) using low-viscosity mono-alcohols as reducing agents, and yet lead to stable colloids.[6] We here demonstrate that using LiOH and NaOH as a base and ethanol (EtOH) as a reducing agent in aqueous media very simply leads at RT to stable and size-controlled surfactant-free colloidal Au and Au-based NPs that are stable for months. We believe that the lack of a detailed study of RT surfactant-free syntheses of Au NPs to date accounts for the overlooked potentials of the promising and surprisingly simple synthesis approach with the combined benefits (i−iv) reported here.

We first provide a detailed account of overlooked parameters in the literature regarding surfactant-free and RT synthesis of Au NPs. We then show the crucial importance of several experimental parameters that severely impact the properties of the resulting NPs. We finally give the first examples of the promising range of applications of this new synthesis to address the remaining challenges in studies and applications of Au-based nanomaterials.

EXPERIMENTAL SECTION

Chemicals. All chemicals were used as received: $HAuCl_4·3H_2O$ (Sigma Aldrich), $PdCl_2$ (anhydrous, 60% Pd basis, Aldrich), $H_2PtCl_6·6H_2O$ (99.9%, Alfa Aesar), $OsCl_3$ (Premion, 99.99% metals basis, Alfa Aesar), H_2IrCl_6 (99.9%, Alfa Aesar), $RuCl_3·xH_2O$ (99.9%, Alfa Aesar), LiOH (98%, Alfa Aesar), NaOH (Puriss., Sigma-Aldrich), KOH (ACS reagent, Sigma-Aldrich), CsOH (99.95%, Aldrich), water [Milli-Q, Millipore, resistivity of >18.2 MΩ cm, total organic carbon (TOC) < 5 ppb], methanol (MeOH, 99.8%, VWR), ethanol (EtOH, absolute, VWR), trisodium citrate dehydrate (Na_3Ct, 99%, Alfa Aesar), polyvinylpyrrolidone (PVP, Alfa Aesar, MW of 58 000), H_2SO_4 (96%, Merck, Suprapur), HCl (37%, 37%, EMSURE ACS, ISO, Reag. Ph Eur), and HNO_3 (67%, Normatom VWR).

Syntheses. *Au NPs.* Unless otherwise specified, the experiments were performed at RT (∼22 °C), ambient pressure, and ambient light, with stirring, in air, in closed 15 or 50 mL centrifuge tubes (VWR) made of polypropylene (PP) used as a reactor. $HAuCl_4$ was added from a 20 mM aqueous stock solution. The base (LiOH, NaOH, KOH, or CsOH) was added from a 57 mM aqueous stock solution. Freshly prepared base solutions were preferred. Unless otherwise specified, the base, water, and mono-alcohol (ROH) were mixed in the PP tube, and then the tube was closed with the dedicated cover. The solution was shaken manually or left to stir for few seconds on a magnetic plate with a magnetic stirrer at ambient light and pressure. The required amount of the $HAuCl_4$ solution was then added last under stirring, and the container closed. Although the reaction can be completed in a few hours, the samples were left to react while being stirred for 24 h at ambient light, ambient pressure, and RT before stirring was stopped. Samples for TEM or high-resolution TEM (HRTEM) characterization were prepared after 24 h. The colloidal dispersions were further kept in a fridge at ∼4−5 °C for other characterization, e.g., by ultraviolet−visible (UV−vis), X-ray diffraction (XRD), X-ray photoelectron spectroscopy (XPS), pair distribution function (PDF), and electrochemistry (see below). The stirrers were cleaned with aqua regia [3:1 (v:v) HCl:HNO_3 mixtures, to be handled with care following the related safety procedures in place in the laboratory].[4] As much as possible, a control experiment was performed the same day as a set of experiments investigating the influence of a given parameter. With the approach proposed, it is

https://doi.org/10.1021/acs.chemmater.3c00090
Chem. Mater. 2023, 35, 2173−2190

relatively easy to perform up to 30 syntheses a day, so the experiments are performed under the same RT and ambient light.

Modifications of the general procedure described above are highlighted in the dedicated sections in the Supporting Information. When N_2 was used, the gas was humidified first by bubbling N_2 in a solution of 30 vol % ROH in water. The humidified stream of gas was then bubbled in the synthesis mixture (plastic connections and tubing were used so that no metal was in contact with the solution). To create dark conditions, the samples were covered in aluminum foil. For RT syntheses, the samples were simply left on a stirring plate. For samples subjected to a heat treatment, the same conditions were used but the samples were left to equilibrate at the desired temperature in a water bath for 15 min before the addition of $HAuCl_4$. The samples were left at the desired temperature as indicated for 1 or 0.5 h and then left for 23 or 23.5 h at RT and ambient light, respectively, after the addition of $HAuCl_4$. For the scale-up experiments to 1 L of solution, a glass container cleaned with ∼10 mL of aqua regia and $HAuCl_4$ was added from a 200 mM aqueous solution.

The final concentrations of each chemical and the volume obtained for different syntheses conditions are listed in the tables in the Supporting Information. Note that the volume percentage expressed is the volume percentage before volume contraction upon mixing of the stock solutions, water, and ROH. The concentrations are also expressed before taking into account the volume contraction.

As described below, *in situ* X-ray total scattering (XRTS) was performed to follow the synthesis. For such experiments, a relatively high Au concentration, e.g., 50 mM $HAuCl_4$, is required to obtain a suitable signal.[29,33] Unfortunately, upon addition of $HAuCl_4$ last as it is preferred at a lower $HAuCl_4$ concentration, the reaction proceeds too fast for any measurement to be performed. For these XRTS experiments, 150 mM base and 50 mM $HAuCl_4$ were used, and ROH was added last, unlike the general synthesis experiments, in which $HAuCl_4$ was added last. The stock solution of the base was at 428 mM, and the stock solution of $HAuCl_4$ at 143 mM, both in water. ROH was added to obtain 30 vol % ROH in the final mixture. To comply with the requirement of the measurement, the synthesis was performed in 3 mm diameter NMR (Wildmad, 3 mm outer diameter, 0.27 mm wall thickness, Type 1 Class A) tubes at RT.[30] The time of synthesis is expressed as the time after mixing all of the chemicals, and no data could be acquired for a few minutes, which corresponds to the time needed to start the measurement.

Au_xPd_y and Pd NPs. The synthesis of the Au_xPd_y NMs with different Au and Pd ratios was performed by mixing different amounts of a stock solution of $HAuCl_4$ at 20 mM in water and a stock solution of $PdCl_2$ at 20 mM in EtOH or water. The two precursors were mixed first in the desired ratios and then added to a solution containing the base, water, and ROH so that the final total PM concentration was 0.5 mM. The rest of the synthesis was performed as detailed for Au NPs.

$Au_xPd_yPt_zOs_uIr_vRu_w$ Samples. The synthesis of the $Au_xPd_yPt_zOs_uIr_vRu_w$ NM samples was performed by mixing different amounts of a 20 mM stock solution of $HAuCl_4$, $PdCl_2$, H_2PtCl_6, $OsCl_3$, $RuCl_3$, and H_2IrCl_6 in MeOH or EtOH. The six precursors were first mixed together and then added to a solution containing the base, water, and 30 vol % ROH. The rest of the synthesis was performed as detailed for the Au NPs so that each precursor was at 0.5 mM with a LiOH:Au molar ratio of 4 or 10. Although no stable colloids were obtained, NPs were formed. The materials were washed with water and redispersed in a 30 vol % EtOH aqueous solution so that the final PM concentration based on the nominal amount used from the precursors is 1 mg_{PM} mL^{-1}.

Characterization. *Transmission Electron Microscopy (TEM) and Energy Dispersive X-ray Spectroscopy (EDS).* The as-prepared or supported Au or Au_xPd_y, alternatively the redispersed $Au_xPd_yPt_zOs_uIr_vRu_w$ samples or the latter supported on a support material, were dropped onto carbon films of nickel or copper TEM grids and left to dry at RT before being imaged on a JEOL 2100 instrument operated at 200 kV. The samples were characterized by recording micrographs in at least three randomly selected areas of the grid and at least three different magnifications. The size of the NPs was evaluated using the ImageJ software by measuring at least 30 NPs for the largest NPs (>50 nm) and more typically 100−200 NPs (for smaller NPs) up to 500 NPs in the case of the synthesis performed using mixtures of ROH, for Au_xPd_y NPs and for the [xAu + yPd] sample where the latter is a mixture of presynthesized Au and Pd NPs.

HRTEM and Scanning TEM-EDS (STEM-EDS). HRTEM and STEM-EDS analysis was performed by using a JEOL 3000F microscope equipped with a scan unit and an EDS detector from Oxford Instruments. For STEM-EDS, a nominal probe size of 1 nm and a camera length of 12 cm were used, and the sample holder was tilted 20° toward the EDS detector. M- and L-α peaks were used for both EDS maps and standardless quantification for Au and Pd, respectively. To reduce noise in the HRTEM images of the Pd nanoparticle, an ABSF filter was applied by using a D. R. G. Mitchell plugin for Digital Micrograph. It was found to be unnecessary to filter the HRTEM images of Au NPs. The EDS spectra were acquired on a FEI Talos F200X instrument equipped with a ChemiSTEM system operated at 200 kV using the Velox Software.

UV−vis. UV−vis spectra were acquired with a Lambda 1050 UV/vis/NIR absorption spectrometer (PerkinElmer). A solvent mixture with the same water:ROH ratio as the sample was used as a baseline. The as-prepared solutions (or diluted to a maximum Au concentration of 0.5 mM) were placed in dedicated quartz UV−vis cuvettes for absorption measurements with a 1 cm path length, and spectra recorded from 200 to 800 nm at ∼1 nm s^{-1}. Au NMs show a signal in UV−vis characterization that corresponds to a size-, shape-, and solvent-dependent localized surface plasmon resonance. This spectrum is rich in information but still complex to fully and accurately interpret.[34] In the case of spherical NPs, the position λ_{spr} (wavelength at the surface plasmon resonance) of the maximum absorption peak intensity (A_{spr}) provides information about the size of the NPs. As the NMs grow and/or aggregate, larger features appear at higher wavelengths and the plasmon peak position will shift to higher wavelengths. An absolute comparison of sizes is challenging based on UV−vis characterization only, and displaying all of the spectra reported for this study will be tedious. To be comprehensive, several metrics used in the literature that capture different features of the UV−vis data are reported in the tables below and in the Supporting Information.

λ_{spr} gives an indication of the size of spherical NPs. In a first approximation, if 525 nm < λ_{spr} < 579 nm, a lower λ_{spr} corresponds to smaller NPs, although very small NPs, $\lesssim$3 nm, do not show a pronounced surface plasmon resonance.[35] $\Delta\lambda/\lambda_{spr}$ at 90% of A_{spr}, the relative width at 90% of A_{spr}, gives an evaluation of the broadness of the surface plasmon resonance peak, so indirectly it gives an indication on the broadness of the size distribution.[36] A_{spr}/A_{450} gives an indication of the size of the NMs with a lower value corresponding to smaller NPs, although the related quantitative models were developed in 100% water and are not directly applicable here in a mixture of water and ROH.[35] The relative intensity measured at 400 nm was suggested to indicate the relative amount of Au^0 in the sample and so provides an estimation of the yield of the synthesis.[34] Previous quantitative analyses were performed in 100% water, and the related absolute conversion coefficients to Au NP yield retrieved[34] are not directly applicable here in a mixture of water and ROH. A_{650}/A_{spr} is reported to indicate the extent of aggregation of the NPs.[37,38] The higher this ratio, the more aggregated the NPs; it must be noted that this is technically relevant only if the NPs are characterized by a well-defined plasmon resonance peak. A_{380}/A_{800} is reported to indicate the stability of the colloid and was here used to compare different samples, where the most stable colloids display a higher ratio.[39]

X-ray Diffraction (XRD). X-ray powder diffraction was measured on a Bruker D8 diffractometer with a Cu anode equipped with a Ni filter in Bragg−Brentano geometry. The samples were prepared by drop-casting a dispersion of the NPs onto a microscope slide and washed with water. Each sample was measured from 5° to 80° 2θ for 4 h, and the background measured under the same conditions subtracted from the data.

ζ Potential Measurements. A Litesizer 500 instrument (Anton Paar) was employed using the analysis software Kalliope (Anton

https://doi.org/10.1021/acs.chemmater.3c00090
Chem. Mater. 2023, 35, 2173−2190

Paar). Courtesy of Ms. J. Schröder from the Prof. M. Arenz group (University of Bern, Bern, Switzerland).

X-ray Photoelectron Spectroscopy (XPS). XPS measurements on the Au_xPd_y NPs prepared at RT were performed with a Thermo Scientific Theta Probe employing a monochromatic Al X-ray source (EAl Kα = 1486.6 eV) operating at a base pressure of $<5 \times 10^{-9}$ mbar using an X-ray spot size of 400 μm and pass energies of 50 eV with dwell times of 10 ms and 0.1 eV detection steps. Avantage and CasaXPS softwares were used for quantitative analysis (see details in the Supporting Information).

X-ray Total Scattering (XRTS) and Pair Distribution Function (PDF) Analysis. TS data for Au and Au_xPd_y samples were collected at the DanMAX beamline at the MAX IV Laboratory, Sweden. Data for the Au NPs were also collected using an Empyrean Series 3 instrument with a Ag source. *In situ* measurements of Au NP formation were performed at beamline P21.1 at the Deutsches Electron Synchrotron, DESY. Data for the $Au_xPd_yPt_zOs_uIr_vRu_w$ samples were measured at beamline P02.1, DESY.

Measurements at Beamline DanMAX, MAX IV Laboratory. The colloidal dispersions of Au_xPd_y NPs prepared using a RT synthesis were drop-casted on a Kapton polyimide thin film. XRTS data were collected in transmission geometry using a DECTRIS PILATIUS3 × 2M CdTe detector with a pixel size of 172 μm × 172 μm. A wavelength of 0.3542 Å was used, and the sample−detector distance was determined to be 91.667 mm from calibration of a NIST LaB_6 standard using Fit2D.[40] The two-dimensional (2D) data were furthermore integrated using Dioptas.[41] The exposure time used for each sample was 15 min. The XRTS data were Fourier transformed using the PDFgetX3[42] software, and a Q_{max} of 19.9 $Å^{-1}$ was used to obtain the PDF. TS data for an empty Kapton film were measured for 45 min and used in the background subtraction. Instrumental resolution parameters (Q_{damp} and Q_{broad}) were determined from a LaB_6 standard.

In-House TS Measurements. The data for the Au NPs were collected at a Panalytical Empyrean Series 3 instrument with a Ag source. The measurements were conducted in the Bragg−Brentano geometry using a flat plate sample holder with a Kapton polyimide thin film. Here a wavelength of 0.56 Å and a GaliPIX detector were used. The exposure time was 7.5 h in the 2θ range of 3−56° and 22.5 h in the 2θ range of 54−110°. The XRD data were furthermore analyzed with the Le Bail method using FULLPROF.[43,44]

Measurements at Beamline P21.1, DESY. For *in situ* experiments, the reaction mixture was injected into a NMR tube and the tube placed in a customized setup with an aluminum block suitable for NMR tubes.[30] The samples were measured in the transmission geometry using a Perkin-Elmer flat panel detector with a pixel size of 200 μm × 200 μm, a wavelength of 0.122 Å, and a sample−detector distance of 396 mm. The exposure time was 30 s. A Q_{max} of 18 $Å^{-1}$ was used to obtain the PDF.

Measurements at Beamline P02.1, DESY. $Au_xPd_yPt_zOs_uIr_vRu_w$ samples were loaded on a Kapton polyimide thin film. Data were measured in the transmission geometry with an exposure time of 300 s. A wavelength of 0.20734 Å, a Varex XRD 4343CT detector with a pixel size of 150 μm × 150 μm, and a sample−detector distance of 253.7 mm were used. A Q_{max} of 18 $Å^{-1}$ was furthermore used to obtain the PDF.

Modeling. All PDF modeling was performed using PDFgui.[45] The Au and Pd *fcc* structures in space group $Fm\bar{3}m$ were used as the structural starting model. The refinement was conducted over the time range of 60−120 min, where the *fcc* structure was dominating and an only minimal contribution from the precursor structure was observed.

Electrochemical Measurements (see also sections SP and SV of the Supporting Information). The electrochemical testing was performed in a three-electrode setup using a glassy carbon tip (5 mm diameter) as the working electrode, a saturated calomel electrode (SCE) as the reference electrode, and a carbon rod as the counter electrode in Teflon cells. The voltage expressed versus the SCE (E_{SCE}) was converted to the voltage versus the relative hydrogen electrode (E_{RHE}) using the relationships $E_{RHE} = E_{SCE} + 0.26$ in 0.5 M H_2SO_4 and $E_{RHE} = E_{SCE} + 1.07$ in 1 M KOH. The as-prepared dispersions of Au or Au_xPd_y NPs were dropped directly on the glassy carbon electrode, polished to a mirror finish using alumina paste as previously reported,[46] and left to dry in 6 × 5 μL for a total volume of 30 μL. For the $Au_xPd_yPt_zOs_uIr_vRu_w$ NM samples, 10 μL of the solution deposited in 2 × 5 μL was used because the solution of NPs was concentrated to ∼1 mg_{PM} mL^{-1}.

The electrochemically active surface area (ECSA) of the Au NPs was evaluated by the charge passed under the reduction peak of gold in H_2SO_4 converted to an ECSA using a conversion factor of 386 μC cm^{-2}.[47] The ECSA of Pd NPs was evaluated using the charge passed under the reduction peak of palladium in KOH using a conversion factor of 424 μC cm^{-2}.[32,48] In the case of samples comprising both Au and Pd, the total ECSA was obtained by the sum of the ECSA evaluated for Au and Pd. The mass activity (MA) was evaluated on the basis of the nominal content of Au or PM in the colloidal dispersion. The MA was corrected by a factor of −3% to take into account the fact that for the EtOH:water ratio used [3:7 (v:v)] the volume contraction is ∼3%. The specific activity (SA) was evaluated as SA = MA/ECSA.

The samples were then tested following different protocols. Protocol A: (1) three scans at 50 mV s^{-1} in 0.5 M H_2SO_4 between 0.00 and 1.50 V_{SCE} (0.26−1.76 V_{RHE}), (2) three scans at 50 mV s^{-1} in 1 M KOH between −0.80 and 0.50 V_{SCE} (0.27−1.57 V_{RHE}), and (3) 50 scans at 50 mV s^{-1} in 1 M KOH and 1 M EtOH between −0.80 and 0.50 V_{SCE} (0.27−1.57 V_{RHE}). This protocol includes steps at high potential to best evaluate the ECSA related to Au that is our reference material in this study.[49] Alternatively, and as indicated, a direct characterization using only one step was used. Protocol B: 50 scans at 50 mV s^{-1} in 1 M KOH and 1 M EtOH between −0.80 and 0.50 V_{SCE} (0.27−1.57 V_{RHE}). For chromoamperometry experiments, a different protocol was used. Protocol C: (1) 10 scans at 50 mV s^{-1} in 1 M KOH and 1 M EtOH between −0.80 and 0.20 V_{SCE} (0.27−1.27 V_{RHE}), (2) chromoamperometry in 1 M KOH and 1 M EtOH at −0.20 V_{SCE} (0.87 V_{RHE}), and (3) 10 scans at 50 mV s^{-1} in 1 M KOH and 1 M EtOH between −0.80 and 0.20 V_{SCE} (0.27−1.27 V_{RHE}). For the comparison of the surfactant-free NPs obtained from different ROH species, the electrochemical protocol was used. Protocol D: (1) three scans at 50 mV s^{-1} in 0.5 M H_2SO_4 between 0.50 and 1.50 V_{SCE} (0.76−1.76 V_{RHE}), (2) 25 scans at 50 mV s^{-1} in 1 M KOH and 1 M EtOH between −0.50 and 0.50 V_{SCE} (0.57−1.57 V_{RHE}), and (3) 10 scans at 20 mV s^{-1} in 1 M KOH and 1 M ethylene glycol (EG) between −0.50 and 0.50 V_{SCE} (0.57−1.57 V_{RHE}). For this comparative study of the effect of different ROH species on the electrocatalytic performances, the chromoamperometry experiments reported were performed at 0.20 V_{SCE} (1.27 V_{RHE}).

RESULTS AND DISCUSSION

Overlooked Synthesis Parameters. An overview of the literature in which polyols and mono-alcohols were used as reducing agents to perform surfactant-free RT synthesis of Au NPs is provided in Table S1. For subsequent discussions, it is important to stress and keep in mind a few important points.

(A) The syntheses are preferentially performed using glycerol as the reducing agent. The syntheses are also preferentially performed in the presence of PVP.[18,50,51] It is here shown that none are required.

(B) In one study using glycerol as the reducing agent, the amount of glycerol is found to control the size and to some degree the shape of the NPs, with larger NPs obtained at higher glycerol contents.[52] In another study, while the glycerol content was roughly in the same range, there was little effect on the resulting Au NP size.[15] The differences observed might be related to the very different concentrations of chemicals and so different $NaOH/HAuCl_4$ molar ratio used, varying from 1−10[52] to 400.[15]

https://doi.org/10.1021/acs.chemmater.3c00090
Chem. Mater. 2023, 35, 2173−2190

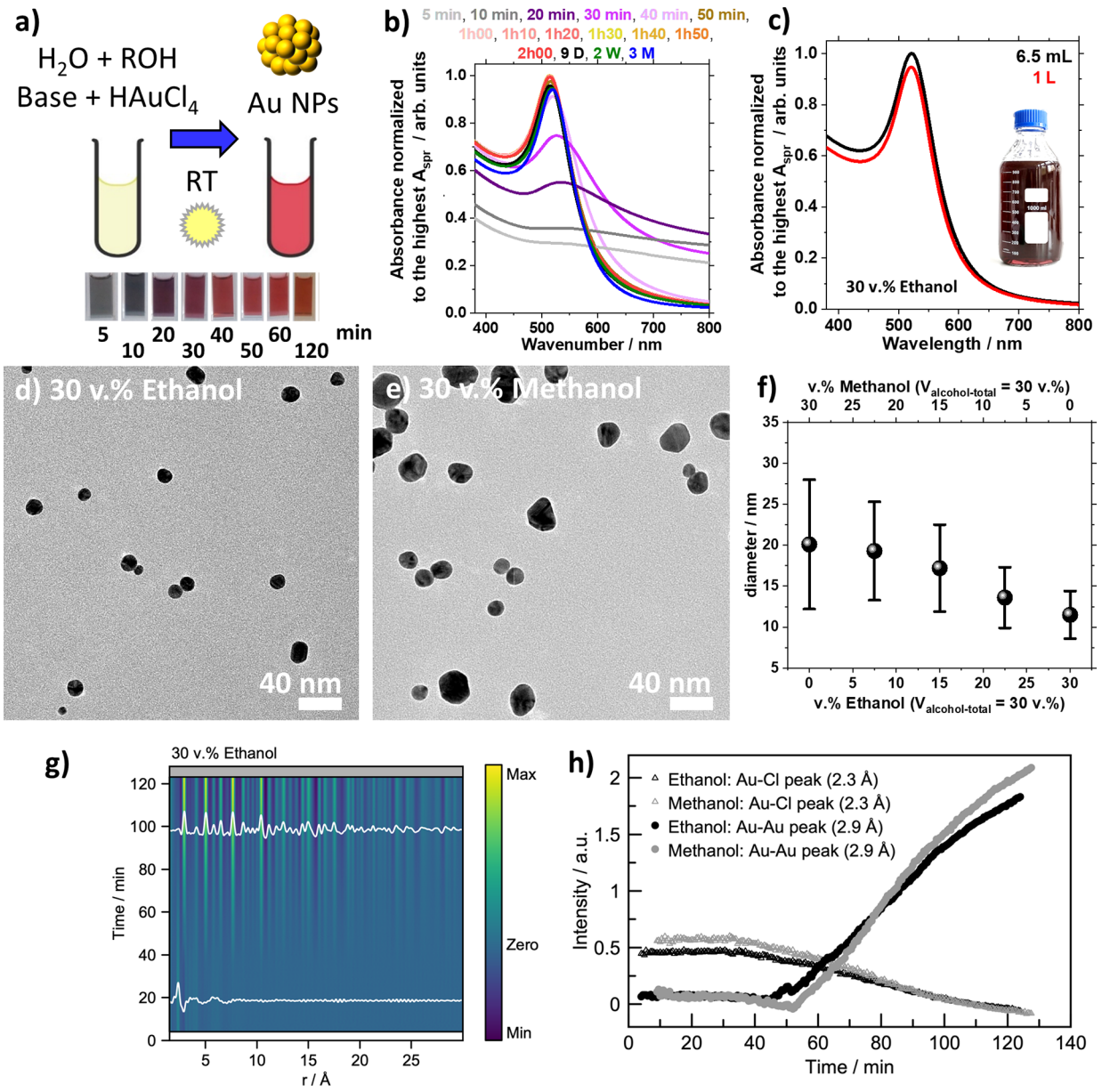

Figure 1. Synthesis and characterization of Au NPs obtained at RT. (a) Schematic representation of the surfactant-free synthesis of Au NPs at RT under ambient light. The bottom image is a collection of pictures of solutions in a UV−vis quartz cuvette with a 1 cm width, for aliquots from a 39 mL solution taken at different times of the synthesis, as indicated, without stirring. (b) Time-resolved UV−vis spectra during Au NP synthesis (min, minutes; h, hours; D, days; M, months). (c) UV−vis spectra of the colloidal Au NPs obtained using NaOH for a total volume of (black) 6.5 mL or (red) 1 L of solution. (d and e) TEM micrographs of Au NPs obtained using ethanol and methanol, respectively. (f) Size retrieved by TEM analysis using different amounts of methanol and ethanol mixed with water. In the experiments depicted in panels a−f, unless specified otherwise, the total volume fraction of alcohol was 30 vol % in water for a total volume of 13 mL, with 2 mM LiOH and $HAuCl_4$ added last for a final concentration of 0.5 mM. The synthesis was performed at RT for at least 24 h with stirring. (g) Time-resolved PDF obtained during the formation of Au NPs using 50 mM $HAuCl_4$ and 150 mM LiOH in 30 vol % ethanol and for the alcohol added last. (h) Time-resolved peak intensity related to the Au−Cl interatomic distance in $HAuCl_4$ and the Au−Au interatomic distance in *fcc* Au NPs as a function of reaction time retrieved from PDF analysis.

(C) High glycerol contents are preferred.[15] This has led to the conclusion that such surfactant-free NPs are mainly stabilized due to the high viscosity of glycerol. This statement is challenged here.

(D) The actual need for polyols was challenged in previous work in which EtOH was used as the reducing agent,[16] but no satisfying control over the synthesis was achieved. In particular, it is not possible to retrieve the concentration of NaOH used in that work. Furthermore, only 10, 50, and 100 vol % EtOH were investigated. This is not the optimal range we identify here because it omits the value of 30 vol % that is here shown to be important for achieving a successful synthesis.

(E) NaOH is the preferred base for the reaction, if not the only one investigated so far.

(F) The order of addition of the chemicals is not necessarily detailed. Also, it is often mentioned that the reactions proceed in few minutes[15,53] or "immediately"[50] upon mixing the reactants, but without more details about how long the experiments were performed. For instance, it is stated in ref 16 that NaOH was added last. We show here that the complete

https://doi.org/10.1021/acs.chemmater.3c00090
Chem. Mater. 2023, 35, 2173−2190

control of the NP structures would actually require specifying various experimental parameters and in particular the time of addition of the base after $HAuCl_4$ and the ROH have been mixed.

(G) There is generally less work on Au-based multimetallic NPs obtained by the surfactant-free approach than on monometallic Au NPs.

In light of the gaps and discrepancies in the literature highlighted above, we investigated in detail the use of mono-alcohols in the RT synthesis of surfactant-free colloidal Au NPs. In particular, we focused on achieving colloidal stability and size control. To comply with the principles of *Green Chemistry*,[54] we optimized the synthesis to minimize the amount of chemicals required to achieve this goal. A specific focus was placed on the use of different alcohols (EtOH and MeOH), different volume percents of alcohols (10−70 vol %), and different bases (LiOH, NaOH, KOH, and CsOH).

Controlled Surfactant-Free Synthesis of Au NPs. To establish if size-controlled Au-based NPs could be obtained by a surfactant-free synthesis in low-boiling point solvents, we investigated a large experimental parameter space, and the influence of each parameter is discussed in the dedicated section of the Supporting Information. The study includes more than 350 experiments to establish the influence of the nature of the alcohol used as the reducing agent (sections SC−SJ), alcohol content (SC and SH), light (SC, SF, and SJ), temperature (SD, SG, SI, and SJ), base concentration (SD and SH), $HAuCl_4$ concentration (SD and SJ), gas atmosphere (SI), the order in which the chemicals are added (SJ and SM), and the nature of the cation in the base (SC, SD, and SG−SJ). Other variables that are found to have a weaker influence of the synthesis are the volume of the solution (SD and SM), stirring (SD), or the type of containers used (SD).

Optimized Synthesis. Mono-alcohols, e.g., EtOH and/or MeOH in alkaline water, are actually suitable reducing agents for obtaining at RT colloidal Au NPs that are stable for months. Figure 1a shows the process taking place during NP formation. Upon addition of $HAuCl_4$ to a mixture of a mono-alcohol, water, and a base, the solutions turn from gray to red, indicative of the formation of small ∼10 nm Au NPs.[8] From the parametric study performed, we found that ∼10 nm Au NPs are easily and reproducibly synthesized from 0.5 mM $HAuCl_4$ and 2 mM LiOH or NaOH in 30 vol % EtOH in water, under ambient conditions, with or without stirring, in polypropylene centrifuge tubes or glassware. There is no need for any extra chemicals such as surfactants.

The particles form in ∼2 h at RT and within a few minutes at 50 °C using EtOH. Figure 1b shows the progressive appearance of a localized surface plasmon resonance (LSPR) during the synthesis, marked by a maximum absorbance intensity around 520 nm in UV−vis measurements, characteristic of small Au NPs. Only minor changes are observed in the UV−vis spectra after ∼2 h at RT, indicative of a relatively fast synthesis. The LSPR and the related peak intensity remain over time for UV−vis measurements conducted after 1, 2, and 3 months, indicative of colloids stable for months in a refrigerator, but also when left on a bench at RT under ambient light. The synthesis is reproducible as discussed in section SL. Figure 1c shows that no large differences are observed between the UV−vis spectra of Au NP dispersions obtained using 6.5 mL or 1 L of solvent. The synthesis thus conveniently scales to 1 L of solution where ∼100 mg of Au NPs can be produced as documented in section SM.

Size and a Certain Degree of Shape Control. A detailed investigation of the parameters allowing size control is given in section SN. EtOH leads to smaller NPs that are ∼10 nm in diameter, as concluded from TEM micrographs in Figure 1d, as opposed to ∼20 nm NPs with MeOH, see Figure 1e. In each case, the Au NPs exhibit the *fcc* structure as seen from XRD diffractograms (Figure S4). The differences in size obtained by using EtOH or MeOH are to be related to the different kinetics of formation observed by following the color change of the dispersion over time. To further follow the reaction, we use *in situ* XRTS with PDF analysis. Refinement of the data can be found in Figures S10 and S11. Time-resolved PDFs are shown in Figure 1g. The PDF represents a histogram of interatomic distances present in the sample and thus allows following structural changes occurring during the reaction. Following the peak intensity of the Au−Cl interatomic distance characteristic of the precursor $HAuCl_4$ and the Au−Au interatomic distance characteristic of *fcc* Au NPs in Figure 1h, the PDFs confirm that the formation of crystalline NPs characterized by a significant increase in the Au−Au peak intensity is slower in MeOH. In simple terms, and assuming that the classical nucleation theory applies here,[55] EtOH is a reducing agent that leads to fast and multiple nucleation events with subsequently moderate growth. MeOH is a less favorable reducing agent, allowing few nucleation events but a slow yet significant growth over time. Conveniently, EtOH is a safe and *green*[10] reducing agent for further scaling (section SM).

Having established that the reducing agent controls NP size, we also show that the size can be tuned using the MeOH:EtOH ratio, as illustrated in Figure 1f. Size control is a general challenge in Au NP synthesis. Typically, concentrations (precursor, surfactants, etc.), time of synthesis, pH, and temperature should all be carefully tuned to control Au NP size.[8] Considering that no surfactants are used here, we achieve a relatively fine size control with relatively uniform size distributions in the range of 10−20 nm using a single parameter, the MeOH:EtOH ratio. Larger NPs are obtained with more MeOH. Because the surfactant-free synthesis proceeds in different alcohols (section SE), this approach opens a range of opportunities to develop further new synthetic strategies.

Formation Pathway and Stabilization. A detailed understanding of the mechanism of formation of Au NPs is ultimately the key to developing complex Au NPs with desirable properties. Despite intense research over the past several decades, the mechanism of formation of Au NPs is still subject to debate, and it is expected that new model systems with unique combinations of features will contribute to solving the remaining challenges.[4,8,56] While a complete understanding of the mechanism at play in NP formation can be the subject of several years of research,[57] e.g., the mechanism of the Turkevich−Frens method reported in 1951 is still debated and investigated[8,58,59] and the synthesis continues to be refined over the years,[60−63] we rationalize the observations reported here by assuming, for now, that the classical nucleation theory applies.[55] To obtain small NPs, it is therefore expected that nucleation events and/or seed formation of Au clusters must be fast relative to the growth of the NPs from these seeds and/or clusters. Accordingly, many seeds and/or nuclei will ultimately grow at the same rate to lead to relatively monodisperse NMs. In contrast, if nucleation events occur over a long period of time, NPs with polydisperse size

https://doi.org/10.1021/acs.chemmater.3c00090
Chem. Mater. 2023, 35, 2173−2190

Table 2. Influence of the EtOH Content and Nature of the Base[a]

ROH	H_2O (vol %)	ROH (vol %)	base	λ_{spr} ($\Delta\lambda/\lambda_{spr}$) nm	A_{spr}/A_{450}	relative yield[b]	A_{650}/A_{spr}	A_{380}/A_{800}	diameter (nm)	PdI
EtOH	90	10	LiOH	523 (6.9%)	1.61	1.00	0.09	32.0	7.5 ± 3.3	0.19
			NaOH	530 (7.0%)	1.75	0.98	0.20	8.20	9.1 ± 6.4	0.49
			KOH	536 (6.9%)	1.82	0.99	0.18	18.4	13.8 ± 5.7	0.17
			CsOH	523 (7.5%)	1.54	1.00	0.16	21.5	10.2 ± 3.8 + network	0.14
	70	30	LiOH	515 (6.6%)	1.53	0.97	0.10	26.3	8.6 ± 2.0	0.05
			NaOH	518 (6.9%)	1.52	0.83	0.10	34.0	8.9 ± 2.2	0.06
			KOH	526 (6.5%)	1.68	0.97	0.16	19.3	13.1 ± 2.9	0.05
			CsOH	534 (12.0%)	1.46	1.00	0.60	2.5	7.6 ± 1.5	0.04
	50	50	LiOH	592 (18.9%)	1.62	1.00	0.92	1.2	>50	X
			NaOH	X	X	X	X	X	X	X
			KOH	554 (15.0%)	1.58	0.3	0.77	1.2	>50	X
			CsOH	X	X	X	X	X	X	X
	30	70	LiOH	X	X	X	X	X	X	X
			NaOH	X	X	X	X	X	X	X
	0	100	LiOH	X	X	X	X	X	X	X

[a]Physical characteristics of the Au NPs obtained using different ROH contents and cations when EtOH is used as the reducing agent. The final concentration of $HAuCl_4$ is 0.5 mM, and the base concentration is 2 mM (base:Au molar ratio of 4) for a volume of 13 mL; the experiments were performed at RT and left to react for 24 h. An X indicates that the measurements could not be performed typically due to the formation of nonstable colloids. See Figure S1 for the definition of a network in this work. [b]Evaluated as the ratio of A_{400} for the sample and the maximum values of A_{400} for the data set at a given volume percent of ROH.

distributions will be obtained. The influence of the most important parameters identified is discussed below.

Influence of the ROH. Certainly, the redox properties of the ROH are an important factor,[11] because the ROH or derived alkoxides play the role of reducing agents.[18] As detailed above, the nature of the ROH used strongly influences the kinetics of the reaction. Larger NPs are obtained using MeOH compared to using EtOH (see Figure 1). However, MeOH and EtOH are not expected to show strong differences in redox potentials.[11] Because the maximum absorbance of a solution of $HAuCl_4$ is shifted in different solvents (see Figure S27), one can expect the $HAuCl_4$ complex to undergo some interaction with the solvent and possibly ligand exchange with methoxy and ethoxy groups.[64] This could explain the Au−O distances probed by PDF (Figure S28). This ultimately accounts for the different resulting materials. In addition, mono-alcohols with higher molecular weights and larger alkyl chains, such as isopropanol and *tert*-butanol, do not lead to small NPs (Figure S6). Another piece of evidence pointing in the direction of the interaction of Au complexes with ROH/RO^- is that using MeOH and adding it last can lead to a large network of Au NMs whereas EtOH leads to NPs (see Figure S21). The properties of the ROH/RO^- species, rationalized as the ability to be oxidized and to interact differently with the Au complex, therefore matter.

Furthermore, when the reaction was performed with glycerol, we observed that a number of rods were obtained (Figure S6), which suggests that despite the challenges in developing surfactant-free syntheses, a certain degree of shape control is possible.

Influence of the ROH Content. We here identified 30 vol % as an optimal value for obtaining small Au NPs. This key value is missing in a previous screening and attempt to use EtOH as the reducing agent.[16] Table 2 lists the properties Au NPs obtained with different volume percents of EtOH (see also section SC for complementary data and results with MeOH). At <30 vol %, no Au NPs form. This corresponds to a case in which there is not enough reducing agent. At higher values, larger NPs, characterized by larger λ_{spr} values, are obtained or no stable colloids, characterized by larger A_{650}/A_{spr} values, are obtained. This corresponds to a case in which there is too much reducing agent. This value hints toward the need for reaching a balance between having enough reducing agent to allow for the reaction to proceed and not having too much reducing agent to avoid overgrowth of the NPs.

Following the *Green Chemistry* principles for the development of NPs,[54] we observed that 30 vol % is also a suitable amount of polyols for the development of surfactant-free syntheses. Furthermore, 35 vol % EtOH was found to be the optimal content in previous studies to favor fast kinetics of reduction, e.g., using sonication.[65] In another study using plasma synthesis,[66] faster kinetics of reduction were observed for a mole fraction of ROH around ∼0.09. Note that 30 vol % ROH corresponds to a mole fraction of ∼0.11. At these values, the interaction of water with ROH changes at the microscopic level. In light of the discussion in Influence of ROH, this physical phenomenon may also influence the reduction mechanism.

Influence of Light. We also observed that light had an influence on the properties of the resulting NPs (see sections SC, SF, and SJ). When the synthesis is performed in the dark, the NPs tend to form slower, and this leads to larger NPs. The influence of light and the need for ROH for the synthesis to proceed suggest that the formation of radicals plays a role in the reduction process.[67]

Influence of the Temperature. To partially alleviate the influence of light, we investigated the effect of temperature on the resulting Au NPs (see sections SD, SG, SI, and SJ). As the temperature increases, the time needed to observe the formation of red colloidal Au NPs decreases. However, we did not observe a significant improvement over the resulting size of the NPs. Above 50 °C, no stable colloids were obtained using EtOH. This suggests that the stabilization of the Au NPs becomes too weak and/or the reducing power of the ROH becomes too strong as the temperature increases.

Influence of the Base Concentration. We now turn to the effect of pH, a parameter typically tuned in the synthesis of Au NPs[8,16] and other PMs,[68] although it was shown to have little

https://doi.org/10.1021/acs.chemmater.3c00090
Chem. Mater. 2023, 35, 2173−2190

Table 3. Influence of the Base:Au Molar Ratio[a]

ROH[b]	H_2O (vol %)[b]	ROH (vol %)[b]	LiOH:Au molar ratio	λ_{spr} ($\Delta\lambda/\lambda_{spr}$) nm	A_{spr}/A_{450}	relative yield[b]	A_{650}/A_{spr}	A_{380}/A_{800}	diameter (nm)	PdI
EtOH	70	30	2	542 (6.6%)	2.02	0.52	0.19	20.9	>100	X
			3	539 (8.0%)	1.84	1.00	0.17	18.6	>40	X
			3.5	523 (6.4%)	1.69	0.90	0.09	35.4	11.7 ± 3.5	0.09
			4	523 (6.5%)	1.63	0.85	0.17	29.4	9.3 ± 2.8	0.09
				517 (6.6%)	1.55	0.88	0.17	12.0	9.2 ± 2.6	0.08
				522 (6.7%)	1.65	0.76	0.17	16.6	8.5 ± 2.1	0.06
			4.5	539 (12.2%)	1.48	0.50	0.52	4.6	7.6 ± 2.6 (not spherical)	0.12
			5	543 (12.2%)	1.48	0.44	0.48	4.9	7.6 ± 3.9 (not spherical)	0.26
			6	549 (15.6%)	1.39	0.49	0.68	1.9	8.5 ± 2.3 + >100 (not all spherical)	0.07
			8	537 (11.4%)	1.41	0.60	0.50	2.5	7.9 ± 2.7 + >100 (not spherical)	0.12
			10	557 (17.2%)	1.44	0.69	0.77	1.8	7.0 ± 2.6 + >100	0.14

[a]Physical characteristics of the Au NPs obtained using different water contents and cations when EtOH is used as the reducing agent. The final concentration of $HAuCl_4$ is 0.5 mM for a volume of 13 mL, and the experiments were performed for 1 h at 50 °C and left to react further for 23 h. An X indicates that the measurements could not be performed typically due to the formation of nonstable colloids. [b]Evaluated as the ratio of A_{400} for the sample and the maximum values of A_{400} for the data set.

influence in the surfactant-free synthesis of Pt NPs in alkaline mono-alcohols.[28,69] Because we here have alcohol/water mixtures in which the pH is not a well-defined variable, we prefer to quote the expected experimental concentration of the base and therefore the base:Au molar ratio (see Figure S14 and Table S8). The detailed results of the parametric study, including different volume percents, different cations, and different ROHs, are given in section SH. As an illustrative example, we focus here on NPs obtained using EtOH and LiOH, which leads to small ∼10 nm NPs. The influence of the base concentration was evaluated using a 1 h step at 50 °C, to limit the possible effects of light that may arise from different kinetics of reaction observed at RT when using different base concentrations. Table 3 lists the results obtained with 30 vol % EtOH. The trends observed are consistent with observations for different volume percents of ROH and different bases.

The optimal dispersion characterized by low λ_{spr}, low $\Delta\lambda/\lambda$, and low PdI values, indicative of small NPs in the absence of different NP structures (e.g., absence of *chunky* materials), was obtained around a LiOH:Au molar ratio of 4 leading to NPs that were ∼10 nm in diameter. For lower LiOH:Au molar ratios, larger NPs were obtained. A LiOH:Au molar ratio of 3.5 led to ∼11 nm NPs. At overly low LiOH:Au molar ratios, the structures were large and not well defined (LiOH:Au molar ratio of 2−3) and showed poor colloidal stability. At higher LiOH:Au molar ratios, i.e., 4.5−5/6, while some NPs were still small, they did not show a spherical shape, which can explain the larger λ_{spr} recorded, and as the ratio increased, larger structures could be observed on the TEM grids (see Figure S15), in agreement with the shift of the λ_{spr} to a higher wavelength.

An optimal value of ∼4 for the base:$HAuCl_4$ molar ratio was probably overlooked in previous studies (see Table S1 and Overlooked Synthesis Paramaters). This partially accounts for the fact that only relatively large NPs were obtained,[16] and the approach was disregarded for the development of a very simple synthesis of surfactant-free colloidal NPs, as achieved herein. A base ratio of 4−5 was shown to be a key threshold in the formation of Au NPs in previous work using MeOH as the solvent but in a synthesis using PVP.[70] UV−vis data in that study showed an increase in the plasmon resonance at 525 nm for this ratio, related to an increased number of Au NPs. The importance of this ratio of 4 between the molar quantities of the base and Au is best understood in light of the equation for the formation of Au NPs (Au^0), further detailed in section SK:

$$2HAuCl_4 + 3H_3CCH_2OH + 8OH^- \rightarrow 3H_3CCOH + 8H_2O + 2Au^0 + 8Cl^-$$

Interestingly, this ratio of 4 is also suitable for obtaining Au NPs using EG or glycerol (see section SE), which shows that lowe amounts of chemicals (here the base can be used compared to what was reported previously (see Table S1). This result paves the way for further optimization of the polyol-based syntheses. Tuning the base:Au molar ratio therefore gives a relative yet promising degree of size and to some extent shape control.

Influence of the Gas Atmosphere. Although we here aim to develop a simple synthetic method, we investigated the effect of the gas atmosphere using a N_2 purge (see the Experimental Section and the Supporting Information). Smaller NPs (∼7 nm) can be obtained using N_2. Although we do not have a clear understanding of the effect of N_2 at this stage, this could be because acetaldehyde (T_{bp} = 20 °C), a possible oxidation product of EtOH, is removed from the solution by the gas stream as it forms. It could also be that O_2 plays the role of an oxidizing agent and/or favors the formation of radicals from the ROH. Therefore, the N_2 purge will ultimately lead to a different set of reducing agents in solution. While using N_2 leads to a relative size control toward smaller NP sizes, using gases unnecessarily complicates the syntheses at the practical level and increases the cost of the synthesis. Therefore, using N_2 was not considered further.

Influence of the Order of Addition of the Chemicals. As stressed in Overlooked Synthesis Parameters, a crucially missing or not detailed parameter in the synthesis of Au NPs using ROH as reducing agents is the effect of the order of addition of the chemicals. We observed across various experiments from RT to 50 °C that the speed at which the reaction proceeds (marked by the appearance of a gray color) is faster, and the resulting NPs are smaller, as the last added chemical is $HAuCl_4$ < base ≪ ROH (see section SJ for detailed examples, including the use of LiOH, NaOH, EtOH, or MeOH). Table 4 illustrates further these results where a UV−

https://doi.org/10.1021/acs.chemmater.3c00090
Chem. Mater. 2023, 35, 2173−2190

Table 4. Influence of the Order of Addition of the Chemicals[a]

ROH	H_2O (vol %)	ROH (vol %)	added last	λ_{spr} ($\Delta\lambda/\lambda_{spr}$) nm	A_{spr}/A_{450}	relative yield[b]	A_{650}/A_{spr}	A_{380}/A_{800}	diameter (nm)	PdI
EtOH	70	30	$HAuCl_4$	523 (6.4%)	1.69	1.00	0.10	32.3	10.0 ± 3.9	0.16
			LiOH	525 (6.7%)	1.72	0.91	0.11	29.5	15.4 ± 4.3	0.08
			ROH	547 (10.7%)	1.62	0.91	0.61	1.6	>50	X

[a]Physical characteristics of the Au NPs obtained using EtOH as the reducing agent for different chemicals added last. The final concentration of $HAuCl_4$ is 0.5 mM, and the LiOH concentration is 2 mM (LiOH:Au molar ratio of 4) for a volume of 6.5 mL. The experiments were performed 1 h at 50 °C and left to react further for 23 h. An X indicates that the measurements could not be performed. [b]Evaluated as the ratio of A_{400} for the sample and the maximum values of A_{400} for the data set.

vis spectrum with a well-defined plasmon resonance and a tail with a lower absorbance at higher wavelengths is obtained when $HAuCl_4$ is added last. A slight shift toward higher λ_{spr} values indicative of larger NPs is obtained when the base is added last, and a spectrum with larger features at higher wavelengths is obtained when ROH is added last. Because we could not find an investigation of this phenomenon using polyols, we made sure this phenomenon is also observed at RT using EtOH and glycerol (see details in section SJ).

The identity of the intermediate chemical species formed during Au complex reduction is not yet definitively known.[71,72] It is expected that the initial $HAu^{III}Cl_4$ complex, $[Au^{III}Cl_4]^-$ in solution, is in equilibrium with various hydroxyl-substituted species with a general formula of $[AuCl_x(OH)_y]^{n-}$ ($x + y = 4$). For alkaline conditions, the equilibria are shifted toward the formation of more hydroxyl-substituted complexes ($y > 1$). However, the higher the value of y, the less likely the complexes are to be reduced in solution.[73] Nevertheless, it is expected that these hydroxy-substituted complexes can be reduced on preexisting NPs, thus initiating a growth phase.[8]

Under the slightly alkaline conditions used here, it is expected that the gold complex will therefore either not undergo reduction in solution or do so only poorly. Such is the case if the reducing agent is added last; i.e., ROH is added to a solution with an expected large amount of hydroxyl-substituted species and therefore with no or few features related to $HAuCl_4$ at low wavelengths in UV−vis characterization (see Figure S27). A direct consequence is that if more base is used, the equilibria are also more strongly shifted toward the formation of hydroxyl-substituted species, which are expected to form more quickly upon addition of $HAuCl_4$, therefore leading to the formation of fewer seeds that slowly (over)grow, as it is observed at relatively high base:Au molar ratios as discussed in Influence of the Base Concentration.

The key to a successful synthesis is then to allow enough $Au^{III}Cl_4^-$ to reduce upon mixing of the different species. This is here achieved by adding $HAuCl_4$ last[8] to a moderately basic solution. The fast reaction that occurs when $HAuCl_4$ is added last can be interpreted as arising from a favorable situation in which the local pH around the $HAuCl_4$ that has just been added does not become too high during the time scale in which the complex starts to be reduced while the ROH is oxidized, so that no or few $[AuCl_x(OH)_y]^{n-}$ species with $y > 1$ are formed, but rather many seeds and/or nuclei. As a further support of this interpretation, the concentration of the stock solution of $HAuCl_4$ also plays a role and smaller NPs are best obtained using concentrated solutions of $HAuCl_4$ added last (see Figure S23).

The case in which the base is added last is more complex because the ROH alone (without base) can start reducing the $HAuCl_4$ (see Figure S27). Upon addition of a base, the reaction proceeds faster probably on preexisting seeds, leading to rather large NPs. The approach of adding the base last as preferred in previous works[16] would then require controlling the time between mixing ROH and $HAuCl_4$ before adding the base.

Nanoparticle Growth. Once the NPs form, their growth is key to control. TEM characterization of the colloidal dispersion over time confirms that the time needed to obtain NPs increases when MeOH is used compared to EtOH (see section SF). We observed, in agreement with previous reports, the formation of networks.[74] However, these networks are probably artifacts from the TEM sample preparation, the possible residual amount of unreacted $HAuCl_4$, the vacuum, and the high-energy beam. Our UV−vis data, however, point toward a growth of the NPs from smaller seeds, in agreement with recent work.[56] In addition here, *in situ* PDF data suggest a growth of the crystalline domains over time (Figures S9−S11), which also rules out the formation of large crystals that would subsequently shrink in size.

The Turkevich−Frens synthesis has been a preferred model system to date because it "includes only three starting materials":[75] water, Na_3Ct, and $HAuCl_4$. Nevertheless, the rich chemistry of Au and Na_3Ct leaves many questions unanswered.[8] If the Turkevich−Frens method leads to small NPs [typically ∼10 nm (see section SP)] and relatively monodisperse NPs due to the use of surfactants, it is also commonly reported that the method or the use of surfactants leads to other NP shapes such as triangles and rods in small percentages.[62,67] The surfactant-free synthesis presented here, while leading to slightly more polydisperse NPs, did not lead to rods or triangles, as assessed by TEM characterization. Therefore, despite being surfactant-free, the approach presented here leads to a relatively homogeneous product.

Influence of Cations. A last aspect of the formation of the NPs is their stabilization. Previous results obtained with glycerol as the reducing agent suggest that viscosity might be a reason for the stabilization of surfactant-free Au NPs.[15] The achievement here of stable colloidal dispersions without a surfactant in low-viscosity solvents shows that viscosity is not the only and not necessarily the main stabilization mechanism, in agreement with recent results for Pt and Ir NPs obtained in mono-alcohols.[29,76]

Identifying in detail the stabilization mechanism(s) of surfactant-free NPs certainly remains a challenge.[23,77] In ζ potential measurements, the NPs prepared using LiOH show a value of −14.5 or −78 mV when the analysis is performed by inputting water or EtOH, respectively, as the solvent in the data treatment (analysis software, Kalliope, Anton Paar). These results suggest a strong stability of the colloids, in agreement with the long-term stability observed over months and/or after centrifugation. Certainly, electrostatic interactions will play a role in the stabilization of surfactant-free NPs,[78] and this points toward the role of the cations.

https://doi.org/10.1021/acs.chemmater.3c00090
Chem. Mater. 2023, 35, 2173−2190

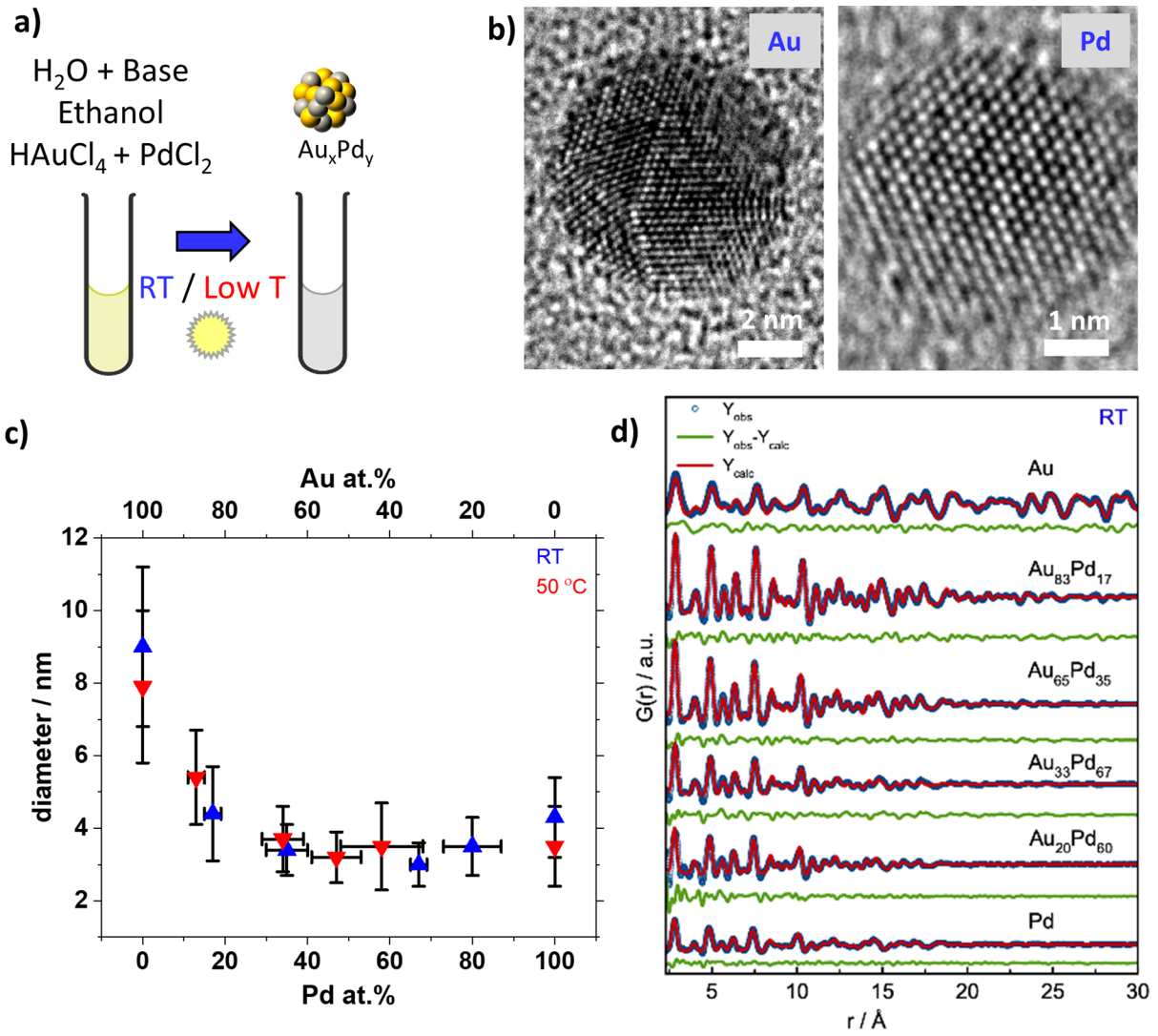

Figure 2. Synthesis and characterization of Au_xPd_y NPs. (a) Schematic representation of the surfactant-free synthesis of Au_xPd_y NPs using alkaline mixtures of ethanol and $HAuCl_4$ and $PdCl_2$ as precursors at RT or 50 °C. (b) Illustrative HRTEM micrographs of Au and Pd NPs obtained at RT. (c) Diameter of the Au_xPd_y NPs evaluated by TEM as a function of their composition evaluated by EDS. (d) XRTS data and PDF refinements using the *fcc* structural model of Au_xPd_y NPs obtained at RT. The NPs were obtained in 30 vol % ethanol in water using 2 mM LiOH and 0.5 mM {$HAuCl_4$ + $PdCl_2$} for a total volume of 13 mL and RT (blue) for a synthesis time of at least 24 h or after low-temperature synthesis (50 °C, red) for 1 h, with stirring.

A complex interplay is likely at play among ROH type, volume percent of ROH, and cations, not to mention the used of additives illustrated in section SO. Overall, LiOH seems to stabilize the NPs better than NaOH or KOH (see Table 2 and section SC), as we also observed for Pt NPs.[76] For a large scale (section SM), NaOH is a cheaper and more promising option than LiOH. The stabilization can be explained by stronger interaction of the smallest cation Li^+ with metal surfaces. The role of Cl^- also cannot be ruled out, nor that of small molecules and solvent interactions.[23,77] The interlinked roles of the ROH, ROH amount, cation, and cation/OH^- concentration are difficult to disentangle at this stage.

Conclusions. Not only the nature of the ROH but also light and the order of addition of the chemicals strongly influence the outcome of the Au NP synthesis. This can be understood considering multiple equilibria between different gold complexes formed, with different redox potentials, and an interplay with the type of ROH used as the reducing agent. It must be kept in mind that as the reaction proceeds, the concentrations of the base will change, as suggested by the equation presented above, further shifting the many chemical equilibria considered.

Interestingly, a certain degree of shape control is achieved from NPs to networks by changing the order of the addition of the chemicals (section SJ) or the base concentration (section SH). The synthesis detailed here therefore offers a range of experimental knobs anticipated to provide new insights into the mechanism(s) of formation of NMs, e.g. regarding the effect of surfactants and/or cations as pointed out in section SO.

We here introduce a new model system with "only" four chemicals: a base, water, $HAuCl_4$, and ROH. However, the rich chemistry already demonstrated suggests that this synthesis can be a suitable model system for further studying Au NP synthesis. Arguably, ROH/RO^- species are ultimately simpler species than Na_3Ct,[58,79] and the fact that the synthesis proceeds here at RT in only a couple of hours is certainly a positive feature for future mechanistic studies.

https://doi.org/10.1021/acs.chemmater.3c00090
Chem. Mater. 2023, 35, 2173−2190

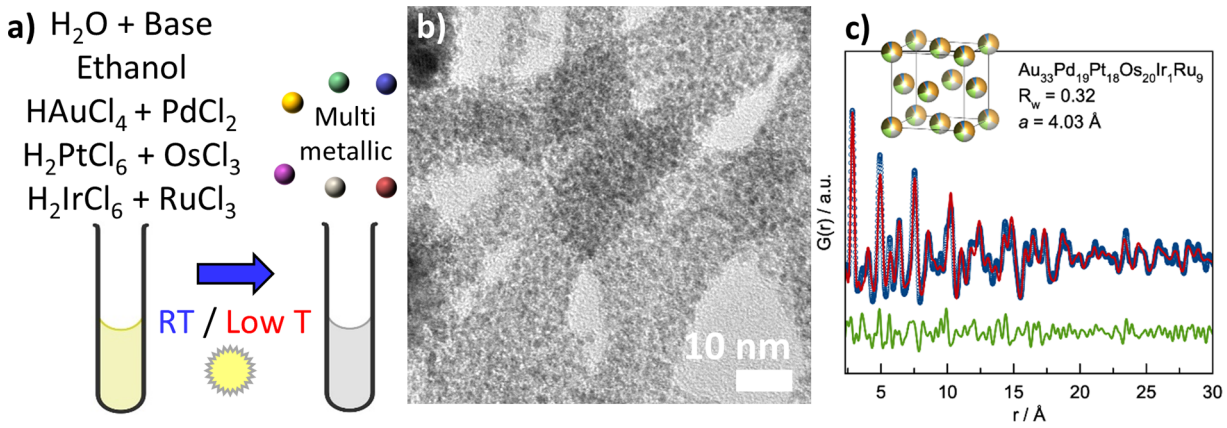

Figure 3. Toward multimetallic NM samples. (a) Schematic representation of the surfactant-free synthesis of $Au_xPd_yPt_zOs_uIr_vRu_w$ NP samples using alkaline mixtures of 30 vol % ethanol and 0.5 mM $HAuCl_4$, 0.5 mM H_2PtCl_6, 0.5 mM $PdCl_2$, 0.5 mM $OsCl_3$, 0.5 mM H_2IrCl_6, and 0.5 mM $RuCl_3$ at RT or 50 °C. (b) TEM micrograph and (c) PDF refinement using the *fcc* structural model for multimetallic samples obtained at RT using LiOH and 30 vol % ethanol where ethanol was added last. The data are colored blue. The fit is colored red. The difference between the data and fit is colored green.

Composition Control. Au NPs are important materials due to their unique properties. Alloying Au with other elements opens an even wider range of opportunities.[80,81] The presented synthesis strategy is suitable for obtaining Au_xPd_y NPs, which have a wide range of applications, as illustrated below for (electro)catalysis. Here, ∼3−4 nm Pd NPs are easily obtained (see Figure 2a,b). The Au:Pd ratio between 0 and 1 is controlled by the Au:Pd precursor ratio. The composition was assessed by TEM-EDS (Figure 2c) and XPS (section SR), and the compositions retrieved from the two techniques agree well. The NP size decreases as the amount of Pd increases (Figure 2c), and PDF characterization confirms that *fcc* structured Au_xPd_y NPs are obtained (Figure 2d).

The synthesis presented is also suitable for RT synthesis of other NPs. Recently, high-entropy alloys (HEAs) made of at least five different elements have received more attention due to their promising catalytic properties.[82,83] The RT synthesis carried out with six different metal precursors (illustrated in Figure 3a) leads to NMs in the size range of 1.5−2.5 nm (see the TEM image in Figure 3b) with the bulk composition $Au_{33}Pd_{19}Pt_{18}Os_{20}Ir_1Ru_9$ estimated by EDS. The presence of $HAuCl_4$ seems to be key for the reaction to proceed at RT. Structural and compositional characterization of individual HEA NPs is a general challenge,[84] and the particles synthesized here are too small for most STEM-EDS equipment for elemental mapping of individual NPs (see the discussion in section SU). PDF analysis confirms small crystalline NPs with a *fcc* structure (Figure 3c). These results show the suitability of the synthesis method proposed to develop Au, Pd, and a range of Au-based NMs.

Electrocatalytic Oxidation of Alcohols. Surfactant-free NPs are relevant for multiple applications and in particular for catalysis in which clean NP surfaces are required.[23,28] As an illustrative example, we use alcohol oxidations, e.g., ethanol (EOR) and glycerol (EGOR) electro-oxidation reactions, that are key reactions at the anode of direct alcohol fuel cells envisioned to enable more sustainable energy conversion.[83,85] To develop optimal electrodes, the mass activity of the catalyst (MA, current retrieved from the oxidation process normalized by the mass of PMs), the electrochemically active surface area (ECSA, measure of the catalytically active surface), the specific activity (SA, activity per electrochemically active surface area), and the stability of the catalyst must be improved.

Representative cyclic voltammograms of the EOR catalyzed by Au NPs are reported in Figure 4a (see also Figure 5). A high current intensity related to alcohol oxidation in the forward (F) scan around 1.1−1.2 V_{RHE} is desirable, and a high ratio of this current to the current in the backward (B) scan around 1.0−1.1 V_{RHE}, related to the oxidation of poisoning species, is indicative of the desirable poisoning resistance to detrimental intermediates formed during alcohol oxidation.[49,85]

Benefits of Surfactant-Free NPs. First, we investigate the electrochemical properties of the Au NPs and the benefits of surfactant-free NPs (see details in section SP). For catalysis, the NPs are typically supported on a material. This supporting step can be challenging with NPs protected by PVP or Na_3Ct, due to unfavorable interactions between protective agents and the support surface. In contrast, the surfactant-free Au NPs are easily supported on various materials by direct adsorption (e.g., on Al_2O_3) or solvent removal (e.g., on carbon) (see details in section SQ). To allow a fair comparison and avoid any effects of the supporting steps, Au NPs prepared with or without surfactants are here readily deposited on conductive electrodes (section SP).

The use of PVP leads to NPs (7.1 ± 1.5 nm in diameter) smaller than the surfactant-free Au NPs characterized by an average diameter of 8.6 ± 2.0 nm, whereas the NPs obtained using the adapted Turkevich−Frens synthesis are 12.3 ± 1.2 nm in diameter (see Table S19). However, using PVP completely passivates the surface of the NPs and no electrochemical measurements can be performed. This illustrates the benefits of developing surfactant-free approaches. The surfactant-free NPs present an ECSA of 8.2 ± 1.1 $m^2\ g^{-1}$, higher than that for NPs prepared by the Turkevich−Frens method characterized by an ECSA of 7.1 ± 0.4 $m^2\ g^{-1}$. This observation agrees with the smaller size of the surfactant-free NPs and the expectation that ECSA increases when the NP size decreases. The SA for the EOR in alkaline media is also higher for surfactant-free NPs than for NPs prepared using water and Na_3Ct. This is explained by the surfactant-free synthesis allowing a better access to the NP surface. The MA of the NPs, e.g., EGOR in alkaline media, is also higher, and/or

https://doi.org/10.1021/acs.chemmater.3c00090
Chem. Mater. 2023, 35, 2173−2190

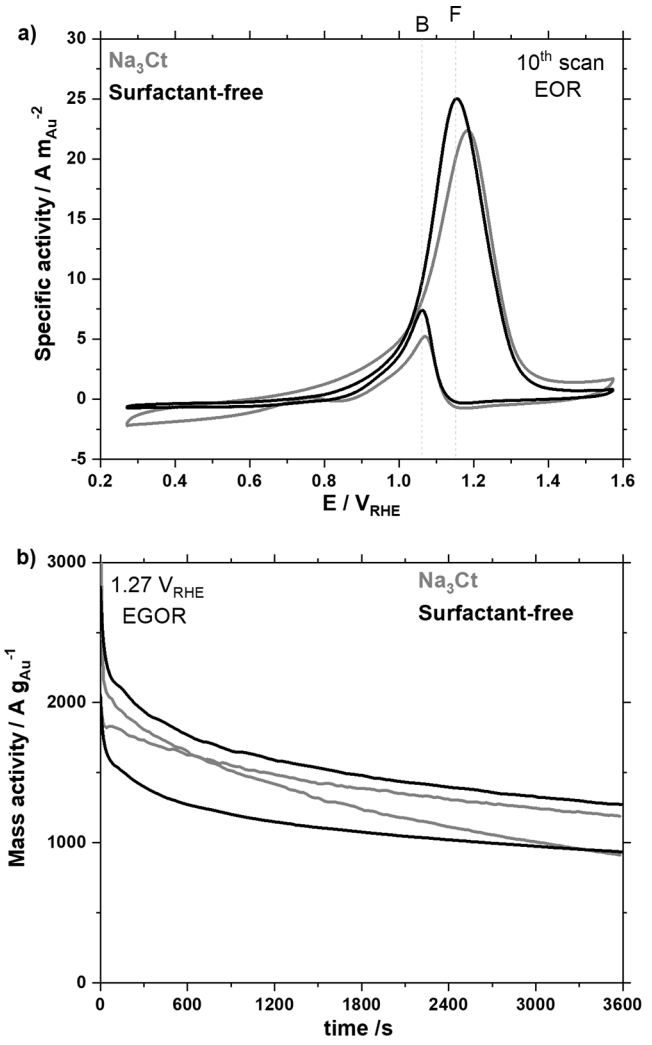

Figure 4. (a) Cyclic voltammograms of Au NPs prepared by the Turkevich−Frens method (Na_3Ct) or without a surfactant (Surfactant-free) for the EOR in alkaline media in 1 M EtOH and 1 M KOH recorded at RT at a scan rate of 50 mV s^{-1}. The 10th scan is displayed. (b) Chronoamperometry of the EGOR performed at 1.27 V_{RHE} for 1 h in 1 M EG and 1 M KOH. NPs prepared with PVP did not show any measurable electrocatalytic activity.

more stable NPs are prepared by a surfactant-free approach. The surfactant-free NPs obtained here also lead to activities that are higher than those of Au NPs obtained using EG or glycerol as the reducing agent (section SP).

The surfactant-free synthesis allows a better access to the NP surface for the reactants, and these results emphasize the benefits of surfactant-free NPs as readily active catalysts without the need for (pre)treatment or washing, avoiding the complications related to extra NP treatments when surfactants or viscous solvents are used.[17]

Influence of Different Composition Control and Different Testing Protocols. The results obtained with Au_xPd_y NPs are summarized in Figure 5 with the illustrative examples of Au, $Au_{83}Pd_{17}$, and Pd NPs for the EOR. Pd NPs show higher catalytic activity at lower overpotentials compared to that of Au NPs for the EOR and EGOR. However, Au NPs show improved stability and better tolerance to poisoning. Developing Au- and Pd-based materials, e.g., Au_xPd_y alloys, is a rewarding strategy for balancing activity, stability, and tolerance to poisoning.[85]

We then characterize the Au_xPd_y NPs (section SR), as illustrated in Figure 5, following two different protocols detailed in the experimental section and summarized in Figure 5b. The ECSA of the NPs increases as the size decreases or as the Pd content increases (Figure 5c). This increase in ECSA correlates with an increase in MA (see, for instance, MAs in Figure 5d, where the NPs were subjected to a relatively harsh protocol A that includes scanning at relatively high potentials). The Au_xPd_y nanocatalysts are more stable (higher MA after harsh treatments) than Pd NPs. Attention is paid to the NMs obtained by the simpler RT synthesis. An optimal NP composition for achieving the highest MA was obtained for ~3.5 nm $Au_{65}Pd_{35}$ NPs (Figure 5e and section ST), in agreement with previous work.[85] These results illustrate the opportunity to tune the properties of surfactant-free Au-based NPs by alloying to easily screen for optimal compositions.

Beyond alloying, and as a further example of the benefits of the simple syntheses reported here, the surfactant-free NMs allow the exploration of two emerging concepts in nanocatalyst design. First, mixtures of different NPs were suggested to enhance catalytic performances compared to those of alloys.[86] These [*x*Au + *y*Pd] nanocomposites lead to MAs comparable to those obtained with Au_xPd_y NPs when the harsher protocol A is used, as summarized in section ST and illustrated in Figure 6a for the most active [40Au + 60Pd]. For protocol B (see Figure 6b), no significant improvement is observed, e.g., compared to Pd NPs. The reason for this enhanced activity in mixtures of NPs is not yet clear; it could originate from the alloying of the two metals during electrochemical testing.[86] Nevertheless, starting with well-defined (surfactant-free) Au and Pd NP batches that are simpler to characterize and mix in the desired ratios is arguably easier, especially at a large scale, than preparing and characterizing the corresponding bimetallic NPs.

Another approach to tuning the NP properties comes with the sample $Au_{33}Pd_{19}Pt_{18}Os_{20}Ir_1Ru_9$ exhibiting different electrochemical properties compared to those of individual Au_xPd_y or [*x*Au + *y*Pd] samples (see further details in section SU). The MA for the EOR remains relatively low due to the large amount of PMs (Figure 6a,b), but an interesting feature of this sample is its resistance to poisoning. Of all of the surfactant-free Pd, Au_xPd_y, [*x*Au + *y*Pd], and $Au_{33}Pd_{19}Pt_{18}Os_{20}Ir_1Ru_9$ NPs characterized here, only the latter showed an improved tolerance to poisoning (see the intensity ratio of forward-to-backward peak intensity of >1.5 in Figure 6d). Although a full understanding of the reasons for this observation is beyond the scope of this first report, the results overall illustrate the promising features of Au-based NMs obtained by the RT synthesis introduced for catalytic studies toward improved NMs.

Comparing NPs obtained by different methods remains a general challenge because the NPs are often characterized by different protocols using, for instance, different electrolyte concentrations, different EtOH concentrations for the EOR, different upper and lower limit potentials, different scan rates, different numbers of scans, different pretreatments in general, and different ink formulations in the case of supported electrocatalysts, not to mention that different normalizations are used to report the results, etc.[27,49,87] Nevertheless, the activity achieved here is relatively high for Au_xPd_y catalysts[88,89] or comparable to that reported elsewhere but using more

https://doi.org/10.1021/acs.chemmater.3c00090
Chem. Mater. 2023, 35, 2173−2190

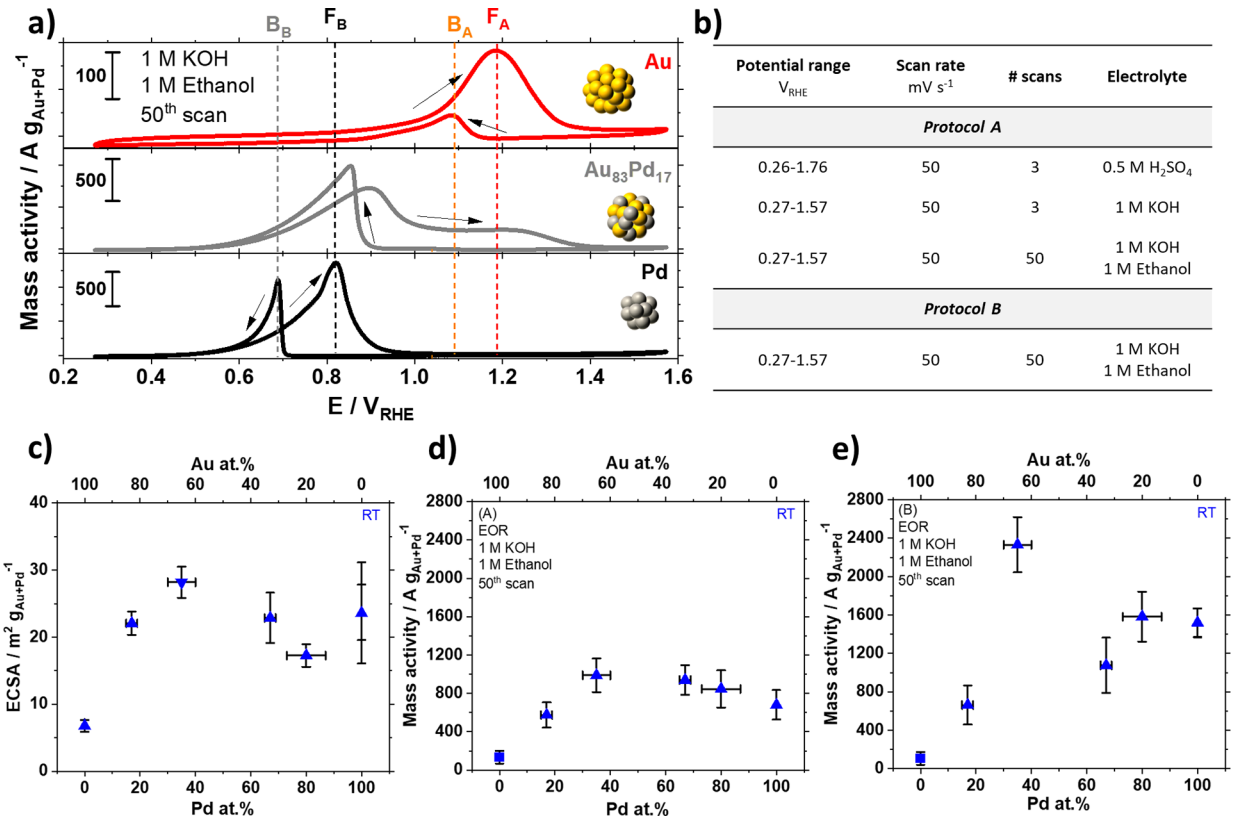

Figure 5. Electrochemical properties of Au_xPd_y NPs as a function of NP composition. Case study of the EOR. (a) Cyclic voltammogram (50th scan) of Au, $Au_{83}Pd_{17}$, and Pd NPs in 1 M KOH and 1 M ethanol recorded at 50 mV s^{-1}, as indicated. The scales used are different to best identify important features. The arrows indicate the forward (F) and backward (B) scans, and the peaks of maximum intensity corresponding to Au (subscript A) and Pd (subscript B) sites are marked by vertical dashed lines. The NPs were characterized following protocol A detailed in panel b. (b) Different characterization protocols used. (c) ECSA estimated following protocol A. (d and e) Mass activity for the EOR estimated following protocols A and B, respectively, detailed in panel b. The NPs were obtained using 2 mM LiOH, 30 vol % ethanol, and different amount of $HAuCl_4$ and $PdCl_2$ for a total concentration of 0.5 mM.

complex synthetic approaches.[85] In this respect, the readily active NPs obtained here by a simple method can be envisioned as a promising reference material for future studies across different laboratories for improved comparative studies.

CONCLUSION

Stable surfactant-free Au NPs are readily obtained by the reduction of $HAuCl_4$ in moderately alkaline mixtures of water and EtOH or MeOH at room or relatively low temperatures (≤50 °C). This approach is a surprisingly simple, straightforward, ultimately cost-effective, and leads to ideal new model systems for the development of surfactant-free yet stable colloidal Au NPs and Au-based multimetallic NMs. The multiple benefits of this simple approach have probably not been exploited to date due to the overlooked influence of several parameters on the synthesis. A reproducible synthetic protocol is here reported after screening of a large experimental parameter space across more than 350 experiments. The strong influence on Au NP synthesis of the mono-alcohol nature and content, base nature, and content as well as the order of addition of the reactants is established. Surfactant-free Au NPs around 10 nm in diameter are easily obtained within 2 h at room temperature by adding $HAuCl_4$ from a concentrated aqueous stock solution to alkaline (NaOH or LiOH) mixtures containing ∼30 vol % EtOH for a final base:$HAuCl_4$ molar ratio of preferably ∼4. The surfactant-free NMs are readily relevant for catalytic applications and studies, e.g., for the EOR, and their performances are better than those of NPs prepared using surfactants or polyols or obtained by the Turkevich–Frens synthesis.

We limit our discussion to a putative formation pathway that we hope will be investigated further and (dis)proved by the community. We document and highlight parameters that we anticipate will be the key to further understanding. (1) One main finding is that the ROH used influences the kinetics of the reduction. (2) A second finding is the critical importance of the order of additions of the chemicals. (3) A third is the influence of light. The NP size distribution and shape remain relatively non-uniform compared to those of most syntheses using surfactants. It is expected that a deeper understanding of the mechanism of formation will help to control even more finely the surfactant-free Au NP properties.

The use of low-boiling point solvents makes the NPs simple to further process, e.g., for supporting steps for heterogeneous catalyst design. The RT synthesis offers opportunities for high throughout, automation, and safe scale-up. The surfactant-free NPs are anticipated to be ideal building blocks for other materials. After 70 years of study and primary focus on the Turkevich–Frens synthesis as the model system for Au NP synthesis, the surfactant-free approach reported here offers new opportunities for education purposes and for fundamental and applied studies of Au-based NMs. It is anticipated that this surfactant-free colloidal synthesis will provide valuable insights into more rational nanomaterial design and syntheses.

https://doi.org/10.1021/acs.chemmater.3c00090
Chem. Mater. 2023, 35, 2173–2190

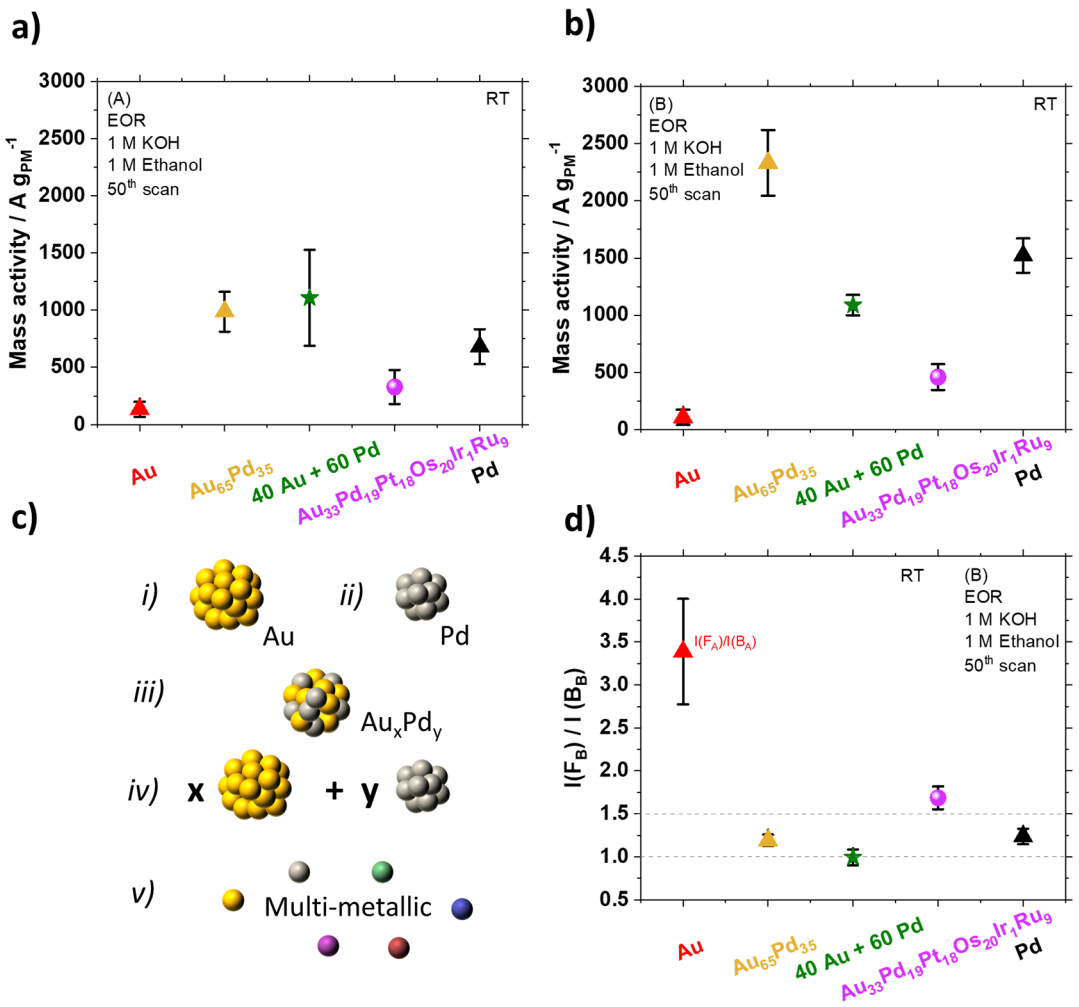

Figure 6. Comparison of different surfactant-free NPs and strategies for electrocatalyst design for the EOR. Au NPs, Pd NPs, the most active Au_xPd_y NPs, i.e., $Au_{65}Pd_{35}$, the most active nanocomposite, i.e., [40Au + 60Pd], and $Au_{33}Pd_{19}Pt_{18}Os_{20}Ir_1Ru_9$ are compared, as indicated. All materials were obtained at RT using LiOH as the base and 30 vol % ethanol. (a and b) Mass activity for the EOR evaluated following protocols A and B, respectively, detailed in Figure 5b. The related materials are schematized in panel c with (i) Au NPs, (ii) Pd NPs, (iii) Au_xPd_y NPs, (iv) nanocomposite [xAu + yPd], and (v) multimetallic samples. (d) Ratio of the forward and backward scan intensity for the highest peak observed in the characterization of the different materials. $I(F_B)/I(B_B)$ was used for all materials expect for Au NPs, for which $I(F_A)/I(B_A)$ was used. The related peaks are illustrated in Figure 5a.

■ ASSOCIATED CONTENT

Supporting Information

The Supporting Information is available free of charge at https://pubs.acs.org/doi/10.1021/acs.chemmater.3c00090.

Materials and Methods, detailed influence of various experimental parameters, and additional characterization of the nanomaterials (PDF)

■ AUTHOR INFORMATION

Corresponding Authors

Jonathan Quinson − *Department of Chemistry, Copenhagen University, DK-2100 Copenhagen, Denmark; Biochemical and Chemical Engineering Department, Aarhus University, DK-8200 Aarhus, Denmark;* orcid.org/0000-0002-9374-9330; Email: jquinson@bce.au.dk

Kirsten M. Ø. Jensen − *Department of Chemistry, Copenhagen University, DK-2100 Copenhagen, Denmark;* orcid.org/0000-0003-0291-217X; Email: kirsten@chem.ku.dk

Authors

Olivia Aalling-Frederiksen − *Department of Chemistry, Copenhagen University, DK-2100 Copenhagen, Denmark;* orcid.org/0000-0003-1462-7173

Waynah L. Dacayan − *Department of Energy Conversion and Storage, Technical University of Denmark, DK-2800 Kgs. Lyngby, Denmark*

Joachim D. Bjerregaard − *Department of Chemistry, Copenhagen University, DK-2100 Copenhagen, Denmark*

Kim D. Jensen − *Department of Chemistry, Copenhagen University, DK-2100 Copenhagen, Denmark;* orcid.org/0000-0001-7466-8458

Mads R. V. Jørgensen − *Department of Chemistry and iNANO, Aarhus University, DK-8000 Aarhus, Denmark; MAX IV Laboratory, Lund University, SE-224 84 Lund, Sweden;* orcid.org/0000-0001-5507-9615

Innokenty Kantor − *MAX IV Laboratory, Lund University, SE-224 84 Lund, Sweden; Department of Physics, The Technical University of Denmark, DK-2800 Kgs. Lyngby, Denmark*

https://doi.org/10.1021/acs.chemmater.3c00090
Chem. Mater. 2023, 35, 2173−2190

Daniel R. Sørensen − *Department of Chemistry and iNANO, Aarhus University, DK-8000 Aarhus, Denmark; MAX IV Laboratory, Lund University, SE-224 84 Lund, Sweden*
Luise Theil Kuhn − *Department of Energy Conversion and Storage, Technical University of Denmark, DK-2800 Kgs. Lyngby, Denmark*
Matthew S. Johnson − *Department of Chemistry, Copenhagen University, DK-2100 Copenhagen, Denmark;* orcid.org/0000-0002-3645-3955
María Escudero-Escribano − *Department of Chemistry, Copenhagen University, DK-2100 Copenhagen, Denmark; Catalan Institute of Nanoscience and Nanotechnology (ICN2), CSIC and BIST, 08193 Barcelona, Spain; ICREA, 08010 Barcelona, Spain;* orcid.org/0000-0002-6432-3015
Søren B. Simonsen − *Department of Energy Conversion and Storage, Technical University of Denmark, DK-2800 Kgs. Lyngby, Denmark;* orcid.org/0000-0001-7172-1225

Complete contact information is available at: https://pubs.acs.org/10.1021/acs.chemmater.3c00090

Author Contributions

The manuscript was written through contributions of all authors. All authors have given approval to the final version of the manuscript. J.Q. designed the work, established the proof of concept, proposed the research direction, and supervised the overall project. J.Q. performed the syntheses and sample preparation for TEM-EDS, HRTEM, XRD, XPS, PDF, ζ potential, UV−vis, and electrochemical characterization. J.Q. performed TEM-EDS, XRD, UV−vis, and electrochemical characterization, data analysis, and interpretation. O.A.-F. helped in the sample preparation for PDF and XPS. O.A.-F. supervised and performed PDF measurements. O.A.-F. performed PDF data analysis and interpretation. O.A.-F. contributed to the draft of the manuscript, in particular the sections related to PDF. W.L.D. and S.B.S. performed the HRTEM data acquisition, analysis, and interpretation and wrote the related sections. J.D.B. performed syntheses. K.D.J. performed XPS data acquisition, analysis, and interpretation and wrote the related sections. M.R.V.J., I.K., and D.R.S. collected XRTS data at DanMAX. L.T.K. helped with TEM data acquisition. M.S.J. supervised J.D.B. M.E.-E. supervised J.Q. and K.D.J. S.B.S. supervised W.L.D. K.M.ØJ. supervised J.Q. and O.A.-F. J.Q., M.E.-E., and K.M.ØJ. finalized the paper. All of the authors discussed the overall results and participated in writing the final version of the manuscript.

Funding

J.Q. acknowledges the European Union's Horizon 2020 research and innovation program under Marie Skłodowska-Curie Grant Agreement 840523 (CoSolCat). M.E.-E. and K.D.J. thank the Independent Research Fund Denmark for the award of a DFF-Research Project 1 grant (9041-00224B). The authors are grateful to the Villum Foundation for financial support through a Villum Young Investigator grant (VKR00015416). Funding from the Danish Ministry of Higher Education and Science through the SMART Lighthouse is gratefully acknowledged. The Danish Research Council (DanScatt) is acknowledged for covering travel expenses for the synchrotron experiments. The authors acknowledge MAX IV Laboratory for time on DanMAX under Proposal 20200731. Research conducted at MAX IV, a Swedish national user facility, is supported by the Swedish Research council under Contract 2018-07152, the Swedish Governmental Agency for Innovation Systems under Contract 2018-04969, and Formas under Contract 2019-02496. DanMAX is funded by NUFI Grant 4059-00009B.

Notes

The authors declare the following competing financial interest(s): The presented nanotechnology is subject to a patent application. Applicant: University of Copenhagen, Denmark; Inventors: J.Q., K.M.Ø.J.; Application number: EP21193770; Status: Patent filed. The general principle of the surfactant-free synthesis is covered by the patent application.

■ ACKNOWLEDGMENTS

Prof. Ib Chorkendorff, Danish Technical University (DTU), is thanked for access to XPS equipment. The authors acknowledge Espen D. Bøjesen (AU), Denmark, for training and facilitating access to the Talos F200X equipment. The authors are grateful to the staff at DESY beamlines P21.1 and P02.1 for support during the experiments. The staff at MAX IV beamline DanMAX are furthermore thanked for the support during remote beamtime.

■ REFERENCES

(1) Ishida, T.; Murayama, T.; Taketoshi, A.; Haruta, M. Importance of Size and Contact Structure of Gold Nanoparticles for the Genesis of Unique Catalytic Processes. *Chem. Rev.* **2020**, *120* (2), 464−525.
(2) Kumari, Y.; Kaur, G.; Kumar, R.; Singh, S. K.; Gulati, M.; Khursheed, R.; Clarisse, A.; Gowthamarajan, K.; Karri, V.; Mahalingam, R.; et al. Gold nanoparticles: New routes across old boundaries. *Adv. Colloid Interface Sci.* **2019**, *274*, 102037.
(3) Li, C. J.; Chai, O. J. H.; Yao, Q. F.; Liu, Z. H.; Wang, L.; Wang, H. J.; Xie, J. P. Electrocatalysis of gold-based nanoparticles and nanoclusters. *Mater. Horiz.* **2021**, *8* (6), 1657−1682.
(4) Daruich De Souza, C.; Ribeiro Nogueira, B.; Rostelato, M. Review of the methodologies used in the synthesis gold nanoparticles by chemical reduction. *J. Alloys Compd.* **2019**, *798*, 714−740.
(5) Nasaruddin, R. R.; Chen, T. K.; Yao, Q. F.; Zang, S. Q.; Xie, J. P. Toward greener synthesis of gold nanomaterials: From biological to biomimetic synthesis. *Coord. Chem. Rev.* **2021**, *426*, 213540.
(6) Gilbertson, L. M.; Zimmerman, J. B.; Plata, D. L.; Hutchison, J. E.; Anastas, P. T. Designing nanomaterials to maximize performance and minimize undesirable implications guided by the Principles of Green Chemistry. *Chem. Soc. Rev.* **2015**, *44* (16), 5758−5777.
(7) Turkevich, J.; Stevenson, P. C.; Hillier, J. A study of the nucleation and growth processe in the synthesis of colloidal gold. *Discuss. Faraday Soc.* **1951**, *11* (11), 55.
(8) Wuithschick, M.; Birnbaum, A.; Witte, S.; Sztucki, M.; Vainio, U.; Pinna, N.; Rademann, K.; Emmerling, F.; Kraehnert, R.; Polte, J. Turkevich in New Robes: Key Questions Answered for the Most Common Gold Nanoparticle Synthesis. *ACS Nano* **2015**, *9* (7), 7052−7071.
(9) Brust, M.; Walker, M.; Bethell, D.; Schiffrin, D. J.; Whyman, R. Synthesis of thio-derivatized gold nanoparticles in a 2-phase liquid-liquid system. *J. Chem. Soc., Chem. Commun.* **1994**, *7*, 801−802.
(10) Prat, D.; Wells, A.; Hayler, J.; Sneddon, H.; McElroy, C. R.; Abou-Shehada, S.; Dunn, P. J. CHEM21 selection guide of classical- and less classical-solvents. *Green Chem.* **2016**, *18* (1), 288−296.
(11) Rodrigues, T. S.; Zhao, M.; Yang, T. H.; Gilroy, K. D.; da Silva, A. G. M.; Camargo, P. H. C.; Xia, Y. N. Synthesis of Colloidal Metal Nanocrystals: A Comprehensive Review on the Reductants. *Chem. Eur. J.* **2018**, *24* (64), 16944−16963.
(12) Yamamoto, H.; Yano, H.; Kouchi, H.; Obora, Y.; Arakawa, R.; Kawasaki, H. N,N-Dimethylformamide-stabilized gold nanoclusters as a catalyst for the reduction of 4-nitrophenol. *Nanoscale* **2012**, *4* (14), 4148−4154.

(13) Khan, T.; Ullah, N.; Khan, M. A.; Mashwani, Z. U. R.; Nadhman, A. Plant-based gold nanoparticles; a comprehensive review of the decade-long research on synthesis, mechanistic aspects and diverse applications. *Adv. Colloid Interface Sci.* **2019**, *272*, 102017.
(14) Ahmed, S.; Annu; Ikram, S.; Yudha, S. S. Biosynthesis of gold nanoparticles: A green approach. *J. Photochem. Photobiol., B* **2016**, *161*, 141−153.
(15) Parveen, R.; Ullah, S.; Sgarbi, R.; Tremiliosi-Filho, G. One-pot ligand-free synthesis of gold nanoparticles: The role of glycerol as reducing-cum-stabilizing agent. *Colloids Surf., A* **2019**, *565*, 162−171.
(16) Junqi, T.; Shiqing, M. Green Synthesis of Colloidal Gold by Ethyl Alcohol and NaOH at Normal Temperature. *Xiyou Jinshu Cailiao Yu Gongcheng* **2013**, *42* (11), 2232−2236.
(17) Hutchison, J. E. The Road to Sustainable Nanotechnology: Challenges, Progress and Opportunities. *ACS Sustain. Chem. Eng.* **2016**, *4* (11), 5907−5914.
(18) Gomes, J. F.; Garcia, A. C.; Ferreira, E. B.; Pires, C.; Oliveira, V. L.; Tremiliosi-Filho, G.; Gasparotto, L. H. S. New insights into the formation mechanism of Ag, Au and AgAu nanoparticles in aqueous alkaline media: alkoxides from alcohols, aldehydes and ketones as universal reducing agents. *Phys. Chem. Chem. Phys.* **2015**, *17* (33), 21683−21693.
(19) Dauthal, P.; Mukhopadhyay, M. Noble Metal Nanoparticles: Plant-Mediated Synthesis, Mechanistic Aspects of Synthesis, and Applications. *Ind. Eng. Chem. Res.* **2016**, *55* (36), 9557−9577.
(20) Liz-Marzan, L. M.; Kagan, C. R.; Millstone, J. E. Reproducibility in Nanocrystal Synthesis? Watch Out for Impurities! *ACS Nano* **2020**, *14* (6), 6359−6361.
(21) Cargnello, M.; Chen, C.; Diroll, B. T.; Doan-Nguyen, V. V. T.; Gorte, R. J.; Murray, C. B. Efficient Removal of Organic Ligands from Supported Nanocrystals by Fast Thermal Annealing Enables Catalytic Studies on Well-Defined Active Phases. *J. Am. Chem. Soc.* **2015**, *137* (21), 6906−6911.
(22) Nicol, J. R.; Dixon, D.; Coulter, J. A. Gold nanoparticle surface functionalization: a necessary requirement in the development of novel nanotherapeutics. *Nanomedicine* **2015**, *10* (8), 1315−1326.
(23) Quinson, J. Surfactant-free precious metal colloidal nanoparticles for catalysis. *Front. Nanotechnol.* **2021**, *3*, 770281.
(24) Schulz-Dobrick, M.; Sarathy, K. V.; Jansen, M. Surfactant-free synthesis and functionalization of gold nanoparticles. *J. Am. Chem. Soc.* **2005**, *127* (37), 12816−12817.
(25) Kawasaki, H. Surfactant-free solution-based synthesis of metallic nanoparticles toward efficient use of the nanoparticles' surfaces and their application in catalysis and chemo-/biosensing. *Nanotechnol. Rev.* **2013**, *2* (1), 5−25.
(26) Wang, Y.; Ren, J. W.; Deng, K.; Gui, L. L.; Tang, Y. Q. Preparation of tractable platinum, rhodium, and ruthenium nanoclusters with small particle size in organic media. *Chem. Mater.* **2000**, *12* (6), 1622−1627.
(27) Quinson, J.; Kunz, S.; Arenz, M. Beyond Active Site Design: A Surfactant-Free Toolbox Approach for Optimized Supported Nanoparticle Catalysts. *ChemCatChem* **2021**, *13* (7), 1692−1705.
(28) Quinson, J.; Neumann, S.; Wannmacher, T.; Kacenauskaite, L.; Inaba, M.; Bucher, J.; Bizzotto, F.; Simonsen, S. B.; Theil Kuhn, L.; Bujak, D.; et al. Colloids for Catalysts: A Concept for the Preparation of Superior Catalysts of Industrial Relevance. *Angew. Chem., Int. Ed.* **2018**, *57* (38), 12338−12341.
(29) Mathiesen, J. K.; Quinson, J.; Blaseio, S.; Kjær, E. T. S.; Dworzak, A.; Cooper, S.; Pedersen, J. K.; Wang, B.; Bizzotto, F.; Johanna, S.; et al. Chemical insights on the formation of colloidal iridium nanoparticles from in situ X-ray total scattering: Influence of precursors and cations on the reaction pathway. *J. Am. Chem. Soc.* **2023**, *145* (3), 1769−1782.
(30) Mathiesen, J. K.; Cooper, S. R.; Anker, A. S.; Kinnibrugh, T. L.; Jensen, K. M. Ø.; Quinson, J. Simple Setup Miniaturization with Multiple Benefits for Green Chemistry in Nanoparticle Synthesis. *ACS Omega* **2022**, *7*, 4714−4721.
(31) Juelsholt, M.; Quinson, J.; Kjær, E. T. S.; Wang, B.; Pittkowski, R.; Cooper, S. R.; Kinnibrugh, T. L.; Simonsen, S. B.; Theil Kuhn, L.; Escudero-Escribano.; et al. Surfactant-free syntheses and pair distribution function analysis of osmium nanoparticles. *Beilstein J. Nanotechnol.* **2022**, *13*, 230−235.
(32) Quinson, J.; Simonsen, S. B.; Kuhn, L. T.; Kunz, S.; Arenz, M. Size effect studies in catalysis: a simple surfactant-free synthesis of sub 3 nm Pd nanocatalysts supported on carbon. *RSC Adv.* **2018**, *8* (59), 33794−33797.
(33) Mathiesen, J. K.; Quinson, J.; Dworzak, A.; Vosch, T.; Juelsholt, M.; Kjaer, E. T. S.; Schroder, J.; Kirkensgaard, J. J. K.; Oezaslan, M.; Arenz, M.; et al. Insights from In Situ Studies on the Early Stages of Platinum Nanoparticle Formation. *J. Phys. Chem. Lett.* **2021**, *12* (12), 3224−3231.
(34) Hendel, T.; Wuithschick, M.; Kettemann, F.; Birnbaum, A.; Rademann, K.; Polte, J. In Situ Determination of Colloidal Gold Concentrations with UV-Vis Spectroscopy: Limitations and Perspectives. *Anal. Chem.* **2014**, *86* (22), 11115−11124.
(35) Haiss, W.; Thanh, N. T. K.; Aveyard, J.; Fernig, D. G. Determination of size and concentration of gold nanoparticles from UV-Vis spectra. *Anal. Chem.* **2007**, *79* (11), 4215−4221.
(36) Larm, N. E.; Essner, J. B.; Thon, J. A.; Bhawawet, N.; Adhikari, L.; St. Angelo, S. K.; Baker, G. A. Single Laboratory Experiment Integrating the Synthesis, Optical Characterization, and Nanocatalytic Assessment of Gold Nanoparticles. *J. Chem. Educ.* **2020**, *97* (5), 1454−1459.
(37) Ye, Y. J.; Lv, M. X.; Zhang, X. Y.; Zhang, Y. X. Colorimetric determination of copper(II) ions using gold nanoparticles as a probe. *RSC Adv.* **2015**, *5* (124), 102311−102317.
(38) Agarwal, S.; Mishra, P.; Shivange, G.; Kodipelli, N.; Moros, M.; de la Fuente, J. M.; Anindya, R. Citrate-capped gold nanoparticles for the label-free detection of ubiquitin C-terminal hydrolase-1. *Analyst* **2015**, *140* (4), 1166−1173.
(39) Merk, V.; Rehbock, C.; Becker, F.; Hagemann, U.; Nienhaus, H.; Barcikowski, S. In Situ Non-DLVO Stabilization of Surfactant-Free, Plasmonic Gold Nanoparticles: Effect of Hofmeister's Anions. *Langmuir* **2014**, *30* (15), 4213−4222.
(40) Hammersley, A. P. FIT2D: a multi-purpose data reduction, analysis and visualization program. *J. Appl. Crystallogr.* **2016**, *49*, 646−652.
(41) Prescher, C.; Prakapenka, V. B. DIOPTAS: a program for reduction of two-dimensional X-ray diffraction data and data exploration. *High Press. Res.* **2015**, *35* (3), 223−230.
(42) Juhas, P.; Davis, T.; Farrow, C. L.; Billinge, S. J. L. PDFgetX3: a rapid and highly automatable program for processing powder diffraction data into total scattering pair distribution functions. *J. Appl. Crystallogr.* **2013**, *46*, 560−566.
(43) Rodriguez-Carvajal, J. Recent advances in magnetic-structure determination by neutron powder diffraction. *Phys. B* **1993**, *192* (1−2), 55−69.
(44) Le Bail, A.; Duroy, H.; Fourquet, J. L. Ab-initio structure determination of $LiSbWO_6$ by X-ray powder diffraction. *Mater. Res. Bull.* **1988**, *23* (3), 447−452.
(45) Farrow, C. L.; Juhas, P.; Liu, J. W.; Bryndin, D.; Bozin, E. S.; Bloch, J.; Proffen, T.; Billinge, S. J. L. PDFfit2 and PDFgui: computer programs for studying nanostructure in crystals. *J. Phys.: Condens. Matter* **2007**, *19* (33), 335219.
(46) Inaba, M.; Quinson, J.; Arenz, M. pH matters: The influence of the catalyst ink on the oxygen reduction activity determined in thin film rotating disk electrode measurements. *J. Power Sources* **2017**, *353*, 19−27.
(47) Padayachee, D.; Golovko, V.; Ingham, B.; Marshall, A. T. Influence of particle size on the electrocatalytic oxidation of glycerol over carbon-supported gold nanoparticles. *Electrochim. Acta* **2014**, *120*, 398−407.
(48) Lukaszewski, M.; Soszko, M.; Czerwinski, A. Electrochemical Methods of Real Surface Area Determination of Noble Metal Electrodes - an Overview. *Int. J. Electrochem. Sci.* **2016**, *11* (6), 4442−4469.
(49) Silva, L. S. R.; Almeida, C. V. S.; Meneses, C. T.; Batista, E. A.; Santos, S. F.; Eguiluz, K. I. B.; Salazar-Banda, G. R. AuPd/C core-shell

and alloy nanoparticles with enhanced catalytic activity toward the electro-oxidation of ethanol in alkaline media. *Appl.Catal. B-Environmental.* **2019**, *251*, 313−325.
(50) Gasparotto, L. H. S.; Garcia, A. C.; Gomes, J. F.; Tremiliosi-Filho, G. Electrocatalytic performance of environmentally friendly synthesized gold nanoparticles towards the borohydride electro-oxidation reaction. *J. Power Sources* **2012**, *218*, 73−78.
(51) Harada, M.; Einaga, H. In situ XAFS studies of au particle formation by photoreduction in polymer solutions. *Langmuir* **2007**, *23* (12), 6536−6543.
(52) Nalawade, P.; Mukherjee, T.; Kapoor, S. Green Synthesis of Gold Nanoparticles Using Glycerol as a Reducing Agent. *Adv. Nanopart.* **2013**, *2* (2), 78−86.
(53) Parveen, R.; Tremiliosi-Filho, G. A step ahead towards the green synthesis of monodisperse gold nanoparticles: the use of crude glycerol as a greener and low-cost reducing agent. *RSC Adv.* **2016**, *6* (97), 95210−95219.
(54) Duan, H. H.; Wang, D. S.; Li, Y. D. Green chemistry for nanoparticle synthesis. *Chem. Soc. Rev.* **2015**, *44* (16), 5778−5792.
(55) Thanh, N. T. K.; Maclean, N.; Mahiddine, S. Mechanisms of Nucleation and Growth of Nanoparticles in Solution. *Chem. Rev.* **2014**, *114* (15), 7610−7630.
(56) Panariello, L.; Radhakrishnan, A. N. P.; Papakonstantinou, I.; Parkin, I. P.; Gavriilidis, A. Particle Size Evolution during the Synthesis of Gold Nanoparticles Using In Situ Time-Resolved UV-Vis Spectroscopy: An Experimental and Theoretical Study Unravelling the Effect of Adsorbed Gold Precursor Species. *J. Phys. Chem. C* **2020**, *124* (50), 27662−27672.
(57) Quinson, J.; Jensen, K. M. Ø. From platinum atoms in molecules to colloidal nanoparticles: A review on reduction, nucleation and growth mechanisms. *Adv. Colloid Interface Sci.* **2020**, *286*, 102300.
(58) Al-Johani, H.; Abou-Hamad, E.; Jedidi, A.; Widdifield, C. M.; Viger-Gravel, J.; Sangaru, S. S.; Gajan, D.; Anjum, D. H.; Ould-Chikh, S.; Hedhili, M. N.; et al. The structure and binding mode of citrate in the stabilization of gold nanoparticles. *Nat. Chem.* **2017**, *9* (9), 890−895.
(59) Mendez, E.; Fagundez, P.; Sosa, P.; Gutierrez, M. V.; Botasini, S. Experimental evidences support the existence of an aggregation/disaggregation step in the Turkevich synthesis of gold nanoparticles. *Nanotechnology* **2021**, *32* (4), 045603.
(60) Kimling, J.; Maier, M.; Okenve, B.; Kotaidis, V.; Ballot, H.; Plech, A. Turkevich method for gold nanoparticle synthesis revisited. *J. Phys. Chem. B* **2006**, *110* (32), 15700−15707.
(61) Ojea-Jimenez, I.; Bastus, N. G.; Puntes, V. Influence of the Sequence of the Reagents Addition in the Citrate-Mediated Synthesis of Gold Nanoparticles. *J. Phys. Chem. C* **2011**, *115* (32), 15752−15757.
(62) Schulz, F.; Homolka, T.; Bastus, N. G.; Puntes, V.; Weller, H.; Vossmeyer, T. Little Adjustments Significantly Improve the Turkevich Synthesis of Gold Nanoparticles. *Langmuir* **2014**, *30* (35), 10779−10784.
(63) Huang, H.; du Toit, H.; Besenhard, M. O.; Ben-Jaber, S.; Dobson, P.; Parkin, I.; Gavriilidis, A. Continuous flow synthesis of ultrasmall gold nanoparticles in a microreactor using trisodium citrate and their SERS performance. *Chem. Eng. Sci.* **2018**, *189*, 422−430.
(64) Quinn, M.; Mills, G. Surface-mediated formation of gold particles in basic methanol. *J. Phys. Chem.* **1994**, *98* (39), 9840−9844.
(65) Mihata, A.; Usman, R.; Kurawaki, J. Selective Synthesis of Gold Nanoparticles in Water/Alcohol Binary Solution Systems by Ultrasonic Irradiation. *E-J. Surf. Sci. Nanotechnol.* **2015**, *13*, 427−430.
(66) Sudare, T.; Ueno, T.; Watthanaphanit, A.; Saito, N. Accelerated nanoparticles synthesis in alcohol-water-mixture-based solution plasma. *Phys. Chem. Chem. Phys.* **2015**, *17* (45), 30255−30259.
(67) Harada, M.; Kizaki, S. Formation Mechanism of Gold Nanoparticles Synthesized by Photoreduction in Aqueous Ethanol Solutions of Polymers Using In Situ Quick Scanning X-ray Absorption Fine Structure and Small-Angle X-ray Scattering. *Cryst. Growth Des.* **2016**, *16* (3), 1200−1212.
(68) Quinson, J.; Inaba, M.; Neumann, S.; Swane, A. A.; Bucher, J.; Simonsen, S. B.; Theil Kuhn, L.; Kirkensgaard, J. J. K.; Jensen, K. M. Ø.; Oezaslan, M.; et al. Investigating Particle Size Effects in Catalysis by Applying a Size-Controlled and Surfactant-Free Synthesis of Colloidal Nanoparticles in Alkaline Ethylene Glycol: Case Study of the Oxygen Reduction Reaction on Pt. *ACS Catal.* **2018**, *8* (7), 6627−6635.
(69) Quinson, J.; Kacenauskaite, L.; Bucher, J.; Simonsen, S. B.; Theil Kuhn, L.; Oezaslan, M.; Kunz, S.; Arenz, M. Controlled Synthesis of Surfactant-Free Water-Dispersible Colloidal Platinum Nanoparticles by the Co4Cat Process. *ChemSusChem* **2019**, *12* (6), 1229−1239.
(70) Siiman, O.; Hsu, W. P. Surface-enhanced Raman scaterring (SERS) enhancements and excitation profiles for 3,5-pyridinedicarboxylate and dabsyl aspartate on colloidal gold. *J. Chem. Soc. Faraday Trans. I* **1986**, *82*, 851−867.
(71) Yao, T.; Sun, Z. H.; Li, Y. Y.; Pan, Z. Y.; Wei, H.; Xie, Y.; Nomura, M.; Niwa, Y.; Yan, W. S.; Wu, Z. Y.; et al. Insights into Initial Kinetic Nucleation of Gold Nanocrystals. *J. Am. Chem. Soc.* **2010**, *132* (22), 7696−7701.
(72) Gao, Y. H.; Torrente-Murciano, L. Mechanistic insights of the reduction of gold salts in the Turkevich protocol. *Nanoscale* **2020**, *12* (4), 2740−2751.
(73) Machesky, M. L.; Andrade, W. O.; Rose, A. W. Interactions of gold(III) chloride and elemental gold with peat-derived humic substances. *Chem. Geol.* **1992**, *102* (1−4), 53−71.
(74) Pong, B. K.; Elim, H. I.; Chong, J. X.; Ji, W.; Trout, B. L.; Lee, J. Y. New insights on the nanoparticle growth mechanism in the citrate reduction of Gold(III) salt: Formation of the au nanowire intermediate and its nonlinear optical properties. *J. Phys. Chem. C* **2007**, *111* (17), 6281−6287.
(75) Ji, X.; Song, X.; Li, J.; Bai, Y.; Yang, W.; Peng, X. Size control of gold nanocrystals in citrate reduction: The third role of citrate. *J. Am. Chem. Soc.* **2007**, *129* (45), 13939−13948.
(76) Quinson, J.; Bucher, J.; Simonsen, S. B.; Kuhn, L. T.; Kunz, S.; Arenz, M. Monovalent Alkali Cations: Simple and Eco-Friendly Stabilizers for Surfactant-Free Precious Metal Nanoparticle Colloids. *ACS Sustain. Chem. Eng.* **2019**, *7* (16), 13680−13686.
(77) Schrader, I.; Warneke, J.; Neumann, S.; Grotheer, S.; Swane, A. A.; Kirkensgaard, J. J. K.; Arenz, M.; Kunz, S. Surface Chemistry of "Unprotected" Nanoparticles: A Spectroscopic Investigation on Colloidal Particles. *J. Phys. Chem. C* **2015**, *119* (31), 17655−17661.
(78) Reichenberger, S.; Marzun, G.; Muhler, M.; Barcikowski, S. Perspective of Surfactant-free Colloidal Nanoparticles in Heterogeneous Catalysis. *ChemCatChem* **2019**, *11* (18), 4489−4518.
(79) Franco-Ulloa, S.; Tatulli, G.; Bore, S. L.; Moglianetti, M.; Pompa, P. P.; Cascella, M.; De Vivo, M. Dispersion state phase diagram of citrate-coated metallic nanoparticles in saline solutions. *Nat. Commun.* **2020**, *11* (1), 5422.
(80) Lu, P. Y.; Zhou, J. W.; Hu, Y. K.; Yin, J. W.; Wang, Y. H.; Yu, J. L.; Ma, Y. B.; Zhu, Z. L.; Zeng, Z. Y.; Fan, Z. X. Gold-based nanoalloys: synthetic methods and catalytic applications. *J. Mater. Chem. A* **2021**, *9* (35), 19025−19053.
(81) Zhu, X. J.; Guo, Q. S.; Sun, Y. F.; Chen, S. J.; Wang, J. Q.; Wu, M. M.; Fu, W. Z.; Tang, Y. Q.; Duan, X. Z.; Chen, D.; et al. Optimising surface d charge of AuPd nanoalloy catalysts for enhanced catalytic activity. *Nat. Commun.* **2019**, *10*, 1428.
(82) Batchelor, T. A. A.; Pedersen, J. K.; Winther, S. H.; Castelli, I. E.; Jacobsen, K. W.; Rossmeisl, J. High-Entropy Alloys as a Discovery Platform for Electrocatalysis. *Joule* **2019**, *3*, 834−845.
(83) Wu, D. S.; Kusada, K.; Yamamoto, T.; Toriyama, T.; Matsumura, S.; Kawaguchi, S.; Kubota, Y.; Kitagawa, H. Platinum-Group-Metal High-Entropy-Alloy Nanoparticles. *J. Am. Chem. Soc.* **2020**, *142* (32), 13833−13838.
(84) Yao, Y. G.; Huang, Z. N.; Li, T. Y.; Wang, H.; Liu, Y. F.; Stein, H. S.; Mao, Y. M.; Gao, J. L.; Jiao, M. L.; Dong, Q.; et al. High-throughput, combinatorial synthesis of multimetallic nanoclusters. *Proc. Natl. Acad. Sci. U. S. A.* **2020**, *117* (12), 6316−6322.

https://doi.org/10.1021/acs.chemmater.3c00090
Chem. Mater. 2023, 35, 2173−2190

(85) Lin, H. H.; Muzzio, M.; Wei, K. C.; Zhang, P.; Li, J. R.; Li, N.; Yin, Z. Y.; Su, D.; Sun, S. H. PdAu Alloy Nanoparticles for Ethanol Oxidation in Alkaline Conditions: Enhanced Activity and C1 Pathway Selectivity. *ACS Appl. Energy Mater.* **2019**, *2* (12), 8701−8706.
(86) Du, J.; Quinson, J.; Zhang, D. M.; Wang, B. Y.; Wiberg, G. K. H.; Pittkowski, R. K.; Schroeder, J.; Simonsen, S. B.; Kirkensgaard, J. J. K.; Li, Y.; et al. Nanocomposite Concept for Electrochemical In Situ Preparation of Pt-Au Alloy Nanoparticles for Formic Acid Oxidation. *JACS Au* **2022**, *2* (7), 1757−1768.
(87) Schreyer, O. A. H.øj; Quinson, J.; Escudero-Escribano, M. Toward Overcoming the Challenges in the Comparison of Different Pd Nanocatalysts: Case Study of the Ethanol Oxidation Reaction. *Inorganics* **2020**, *8* (11), 59.
(88) Zhu, L. D.; Zhao, T. S.; Xu, J. B.; Liang, Z. X. Preparation and characterization of carbon-supported sub-monolayer palladium decorated gold nanoparticles for the electro-oxidation of ethanol in alkaline media. *J. Power Sources* **2009**, *187* (1), 80−84.
(89) Liang, Z. X.; Song, L.; Deng, S. Q.; Zhu, Y. M.; Stavitski, E.; Adzic, R. R.; Chen, J. Y.; Wang, J. X. Direct 12-Electron Oxidation of Ethanol on a Ternary Au(core)-PtIr(Shell) Electrocatalyst. *J. Am. Chem. Soc.* **2019**, *141* (24), 9629−9636.

https://doi.org/10.1021/acs.chemmater.3c00090
Chem. Mater. 2023, 35, 2173−2190